American Mineralogist, Volume 104, pages 724–743, 2019

Geochemical characteristics of lawsonite blueschists in tectonic mélange from the Tavşanlı Zone, Turkey: Potential constraints on the origin of Mediterranean potassium-rich magmatism

Yu Wang[1,2,*], Dejan Prelević[3,4], and Stephen F. Foley[2]

[1]State Key Laboratory of Isotope Geochemistry, Guangzhou Institute of Geochemistry, Chinese Academy of Sciences, Guangzhou 510640, China. Orcid 0000-0001-6560-0654
[2]ARC Centre of Excellence for Core to Crust Fluid Systems/GEMOC; Department of Earth and Planetary Sciences, Macquarie University, New South Wales 2109, Australia
[3]Faculty of Mining and Geology, Belgrade University, Đušina 7, 11000 Belgrade, Serbia
[4]Institute for Geosciences, University of Mainz, Becherweg 21, Mainz 55099, Germany

Abstract

The petrology, mineralogy, and geochemistry of lawsonite blueschists from the Tavşanlı zone in northwest Turkey—one of the best-preserved blueschist terranes in the world—have been comprehensively investigated. The blueschist samples contain lawsonite + sodic amphibole + phengite + chlorite + titanite + apatite ± aragonite ± quartz ± relict igneous pyroxene ± Mn-rich garnet and opaque phases. Lawsonite is a significant repository for Sr, Pb, Th, U, and REE, whereas phengite carries the most large-ion lithophile element (LILE), titanite hosts the highest Nb and Ta as well as considerable amounts of high field strength element (HFSE), and apatite strongly controls Sr. Two groups of blueschist have different origins—enriched continent-derived terrigenous origin and mid-ocean ridge basalts (MORB)-like submarine basalts—assigned on the basis of whole-rock major and trace element compositions and initial Sr-Nd-Pb isotopic results. Lawsonite in blueschist with enriched origin exhibits strong Th/La fractionation, raising the possibility of the involvement of blueschist facies mélange to explain the origin of Mediterranean potassium-rich magmatism because similarly high Th/La ratios are also observed in the Mediterranean potassium-rich lavas. We propose that subduction-induced tectonic imbrication took place entirely at shallow depths (<80 km), giving rise to a newly formed lithosphere where oceanic and continental crustal materials, sediments, strongly depleted peridotite blocks, and metamorphic rocks are all imbricated together, and in which many of the compositional characteristics of the lawsonite blueschist are sequestered. Subsequent melting of the fertile and enriched components in this new lithosphere would result in the generation of potassium-rich post-collisional mafic magmas with diagnostic geochemical affinities.

Keywords: Lawsonite blueschist, Sr-Nb-Pb isotope, protolith of blueschist, the Tavşanlı zone, K-rich magmatism, high Th/La

Introduction

Blueschists and eclogites result from subduction along cold geothermal gradients. They provide a natural laboratory to investigate the passage of chemical components from subducting crust to the overlying mantle wedge during subduction, and they help understand the origin of earthquakes that may be triggered by the dehydration and embrittlement of subducting oceanic crust (Ernst 1988; Okay 1989; Maekawa et al. 1993; Maruyama et al. 1996; Fryer et al. 1999; Spandler et al. 2003; Kim et al. 2015; Palin and White 2015; Okazaki and Hirth 2016). It is widely recognized that without knowledge of subduction zone metamorphism, it is impossible to fully examine the compositional heterogeneity of the mantle because metamorphic processes during subduction will dramatically affect mantle metasomatism and subduction-related dynamics (Maekawa et al. 1993; Tribuzio et al. 1996; Poli and Schmidt 1997; Yaxley and Green 1998; Klemme et al. 2002; Tsujimori and Ernst 2014).

As subduction occurs, metamorphic breakdown and dehydration of hydrous minerals may result in melting in the mantle wedge, liberating a substantial amount of trace elements. Blueschist, and to a lesser extent eclogite, are the principal high-pressure low-temperature (HPLT) metamorphic reservoirs of these hydrous minerals (e.g., lawsonite, epidote, phengite, chlorite, and amphibole), documenting many key features of subduction zone metamorphism. Therefore, diverse aspects of their petrological and geochemical characteristics have been extensively studied (e.g., Okay 1980, 1982; Ernst 1988; Tribuzio and Giacomini 2002; Spandler et al. 2003; Volkova et al. 2009; Ukar and Cloos 2015) including the pressure-temperature stability of blueschists, and blueschist-greenschist or blueschist-eclogite transition equilibria and thermodynamics (e.g., Schmidt and Poli 1994; Poli and Schmidt 1997; Martin et al. 2011).

* E-mail: wangyu@gig.ac.cn

0003-004X/19/0005–724$05.00/DOI: https://doi.org/10.2138/am-2019-6818

Despite the usefulness of blueschists to decipher the subduction process, they occur extremely rarely, restricted to subduction of cold oceanic slabs under high-pressure and low-temperature environment. In addition, they must be exhumed rapidly enough to avoid transformation to other facies assemblages (Okay et al. 1998; Agard et al. 2009; Plunder et al. 2015). Numerous works have been carried out on blueschists, mostly along the Mesozoic and Cenozoic orogenic belts of the circum-Pacific and Tethyan regions. Of particular interest are localities in collisional orogenic belts including the Tethyan domains in Eurasia (Mediterranean, Western Alps, east-central China, and Himalaya). Many have contributed specifically to the explanation of the petrogenesis, geochemistry, tectonics, and geodynamics of Turkish blueschists occurring in the Tavşanlı zone (Okay 1980, 1982, 1986, 1989, 2002; Davis and Whitney 2006; Topuz et al. 2008, Seaton et al. 2009; Özbey et al. 2013; Plunder et al. 2013, 2015; Whitney et al. 2014; Martin et al. 2014; Mulcahy et al. 2014; Pagé et al. 2016). However, no systematic work has been done regarding the whole-rock and mineral trace element compositions, and especially isotopic constraints of the Tavşanlı zone blueschists.

Furthermore, the potential of blueschist facies mélange in deciphering the origin of Mediterranean potassium-rich magmatism is rarely acknowledged. Mélanges with matrices consisting of either clastic sedimentary rock or ophiolitic rock have been recognized in orogenic belts worldwide (Raymond 1984; Cloos and Shreve 1988; Parkinson 1996; Collins and Robertson 1997; Harris et al. 1998; Fotoohi Rad et al. 2005; King et al. 2006; Bulle et al. 2010; Guo et al. 2014; Ukar and Cloos 2015). They are typically created in the accretionary wedge above a subduction zone where blueschist-facies rocks are underlain by, or imbricated with, several different lithologies. Along the Alpine-Himalayan orogenic belt (AHOB), especially in the Mediterranean and Turkey, mélanges that include Cretaceous blueschist have been described widely (e.g., Collins and Robertson 1997; Tankut et al. 1998; Rojay et al. 2004; Tsujimori et al. 2006; Göncüoglu et al. 2006, 2010; Çetinkaplan et al. 2008; Plunder et al. 2013, 2015; Çelik et al. 2016). It has been proposed recently that blueschist facies mélange might help to understand the geodynamics and compositions of post-collisional potassium-rich AHOB magmatism (e.g., Tommasini et al. 2011; Prelević et al. 2013; Wang et al. 2017). A recent study showed that some lawsonite in the Tavşanlı zone blueschists contains critical trace element characteristics—extremely high Th/La ratios—which might be utilized to decipher the origin of AHOB potassium-rich lavas (Wang et al. 2017). In addition, various geochemical proxies imply an important role for sediments in the source of Mediterranean K-rich lavas (Conticelli 1998; Conticelli et al. 2002; Peccerillo and Martinotti 2006; Prelević et al. 2008; Tommasini et al. 2011). Subduction in western Turkey at ~95–90 Ma furnished the base of the Anatolide-Tauride block with sediments and oceanic rocks until the Izmir-Ankara-Erzican suture was sealed by Eocene plutonism (Van Hinsbergen 2010; Mulcahy et al. 2014; Fornash et al. 2016). Therefore, it is essential to scrutinize the tectonically imbricated mélange as it carries critical yet complex information about oceanic and continental crustal materials, sediments, strongly depleted peridotite blocks, and metamorphic rocks including blueschists, which may be potential source materials for Mediterranean and AHOB potassium-rich post-collisional magmas.

This contribution aims to (1) present a comprehensive set of mineralogical, petrological, and geochemical results on representative lawsonite blueschist samples from the Tavşanlı zone, Turkey, (2) to constrain the nature of the protoliths of the Tavşanlı zone blueschist, and (3) to propose a feasible solution to account for the characteristic Th/La conundrum of Mediterranean K-rich magmas.

Geological setting

The geological background of Western Anatolia and the Tavşanlı zone is detailed in several publications (e.g., Şengör and Yılmaz 1981; Okay and Tüysüz, 1999; Pourteau et al. 2010, 2013; Plunder et al. 2013, 2015). Only essential information is outlined here; the reader is referred to Okay and Whitney (2010) and Plunder et al. (2013, 2015) for further details on local geology and tectonic evolution.

The Tavşanlı Zone lies south of the Alpine Izmir-Ankara-Erzican suture that marks the closure of the Neotethyan Ocean, dividing Western Anatolia into two major blocks, the Pontides and the Anatolides-Taurides (Şengör and Yılmaz 1981; Okay and Whitney 2010). The crust of western Anatolia originated by accretion of numerous continental slivers and island arcs beginning in the Early Mesozoic, and is subdivided into three regions, the Tavşanlı Zone (with length of ~250 km and width of 50–60 km) in the north, the Menderes Massif to the southwest, and the Afyon Zone to the northeast of the Menderes Massif (e.g., Okay and Tüysüz 1999; Altunkaynak and Genç 2008; Plunder et al. 2013; Fig. 1a). These comprise the most important metamorphic zones in Gondwana-derived continental domains. The Tavşanlı Zone is commonly recognized as a belt of blueschists tectonically overlain by an oceanic accretionary complex and large peridotite slabs later intruded by the undeformed Early to Middle Eocene granodiorites (Okay and Whitney 2010). The Tavşanlı Zone blueschists mark the subducted north-facing passive continental margin of the Anatolide-Tauride Block and illustrate an analogous tectonic evolution to those from Oman (e.g., Goffe et al. 1988; Searle et al. 1994).

There are three major units in the Tavşanlı Zone: the lower Orhaneli blueschist sequence (where samples in this study were collected), a Cretaceous accretionary mélange derived from the Tethyan Ocean in the middle, and an upper obducted ophiolitic thrust sheet. The Orhaneli sequence constitutes a coherent stratigraphic series consisting mainly of three major formations of metasedimentary rocks; the Kocasu Formation (metaclastic rocks) at the base, the İnönü Formation (marble) in the middle and the upper Devlez Formation (mostly metabasite) where the samples in this study were collected (Okay and Whitney 2010; Plunder et al. 2015, 2016; Fig. 1b). The Devlez Formation comprises metabasites, metacherts, and phyllites with metabasites constituting >80% of the Formation with a structural thickness of ~1 km to the northeast of Tavşanlı.

Our samples were collected between the villages of Göynücek and Dodurga (coordinates see Table 1) where excellent outcrops of the blueschists of the Devlez Formation are exposed (Fig. 1c). Here, the blueschist outcrops consisted of a sequence of intercalated metabasite, metachert, metashale, and metagabbro blocks of different size from 100 to 10 m in diameter, immersed in a mélange matrix (Fig. 2a). The selected samples were collected from two locations that represented

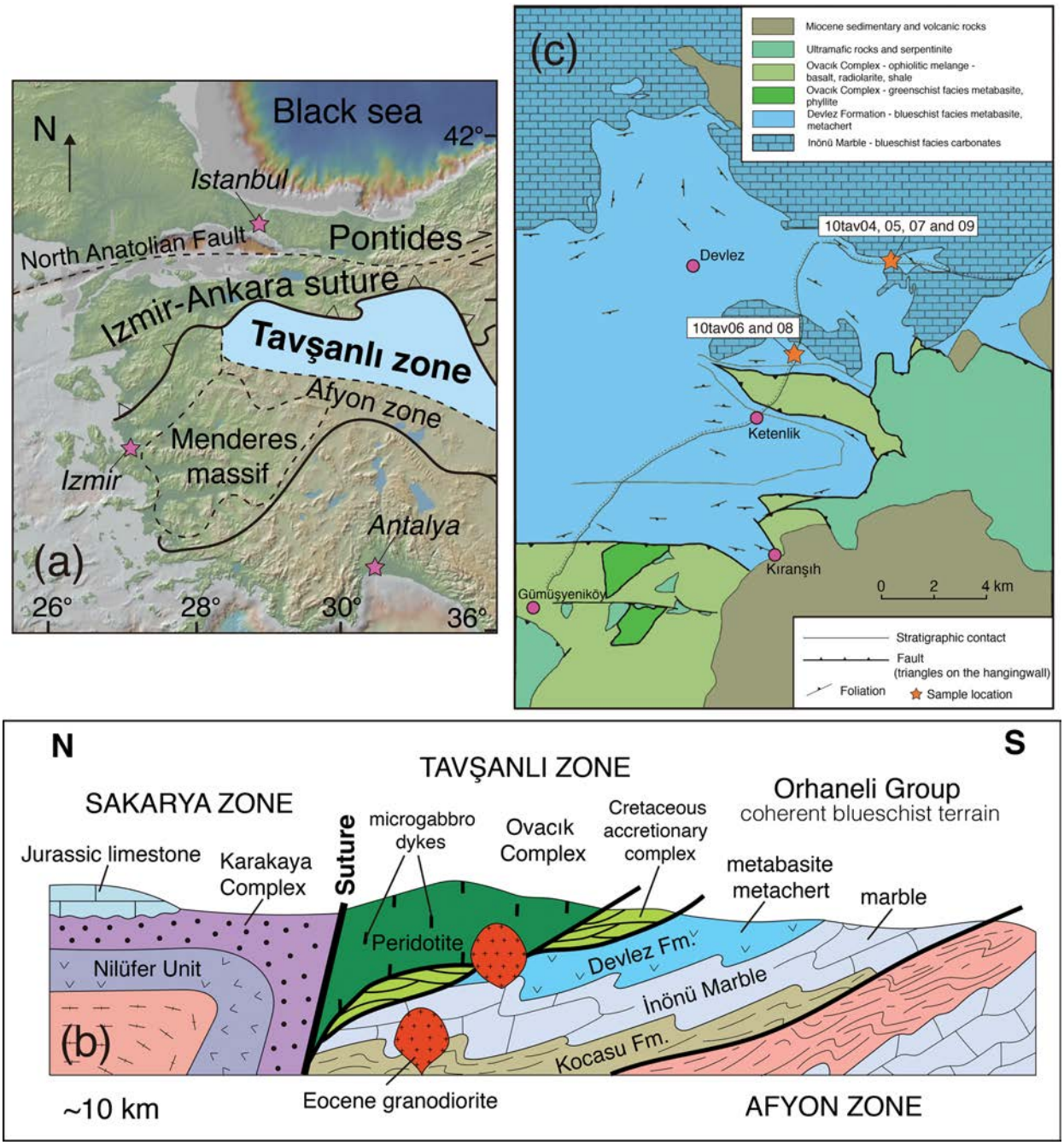

Figure 1. (**a**) Tectonic map of western Anatolia showing the position of the Tavşanlı zone (blue). Modified from Plunder et al. (2015). Topography of this area from Geomapapp 3.3.6 (http://www.geomapapp.org/). (**b**) Simplified schematic cross-section across the Tavşanlı zone showing tectonostratigraphic units and structure (not to scale). Note the three major formations in the Orhaneli Group: Kocasu Formation (metaclastic rocks) at the base, the İnönü Marble in the middle and the upper Devlez Formation (metabasite and metachert) where the samples in this study were collected. Modified from Okay and Whitney (2010). (**c**) Geological map of the region northeast of Tavşanlı showing the locations of the samples (orange stars). Modified from Okay and Whitney (2010). (Color online.)

larger blocks of blueschists (Figs. 1b, 2b, and 2c). These metabasites are characterized by a typical paragenesis of sodic amphibole, lawsonite, chlorite, titanite, and phengite, which are commonly recognized as the classical "blue" blueschists (Okay 1980a; Okay and Whitney 2010). They have been completely recrystallized from possibly submarine lavas, pyroclastic rocks, and tuffs with the growth of a penetrative metamorphic fabric and new minerals. A strong foliation and mineral lineation in metabasites and metacherts are defined by the parallel alignment of sodic amphibole grains. The age of the blueschist

metamorphism, based on Rb/Sr phengite dating, is Campanian (~80 Ma, Sherlock et al. 1999), whereas in a recent in situ $^{40}Ar/^{39}Ar$ phengite dating study (Fornash et al. 2016) ages of 90–93 and 82 ± 2 Ma were interpreted as the ages of peak and retrograde metamorphism, respectively. Details of analytical techniques, seven Supplemental figures and all the data for this paper are available in Supplemental[1] Information S1 and S2.

Results

The six selected mafic blueschist samples are schistose and finely crystalline. Sodic amphibole, lawsonite, and chlorite are the most common phases in all six samples, making up 60–80% of the rock. Except for samples 10tav04 and 05, there is no evidence of extensive metasomatism as only low-grade incipiently high pressure metamorphosed rocks have been reported to show considerable metasomatism effects in the Tavşanlı zone (Okay 1982). Backscattered SEM images of all samples are shown in Figure 3, and their parageneses are listed in Table 1.

Sample description

10tav04. Sample 10tav04 is a lawsonite blueschist composed of lawsonite, sodic amphibole, pyroxene, phengite,

Table 1. Mineral assemblages and mineral modal abundances of blueschist samples

Sample	Location	Coordinates	Mineral assemblage (mode %)
10tav04	Tavşanlı Zone, Turkey	39°43′49.72″N; 29°49′19.93″E	Amp (26), Chl (24), Phen (18), Law (8), Tnt (6), Arg (6), Cpx (5), Apa (5), *Py, Hem*
10tav05	Tavşanlı Zone, Turkey	39°43′49.72″N; 29°49′19.93″E	Chl (26), Amp (18), Law (15), Arg (12), Qrz (8), Phen (8), Apa (6), Tnt (3), *Ga*
10tav06	Tavşanlı Zone, Turkey	39°45′27.23″N; 29°50′53.70″E	Amp (30), Law (25), Chl (14), Arg (8), Phen (7), Apa (6), Tnt (4), Qrz (4), *Py, Hem*
10tav07	Tavşanlı Zone, Turkey	39°43′49.72″N; 29°49′19.93″E	Amp (30), Law (25), Qrz (15), Phen (10), Chl (8), Arg (8), Apa (6), Tnt (3), Mn-Grt (1), *Py, Hem*
10tav08	Tavşanlı Zone, Turkey	39°45′27.23″N; 29°50′53.70″E	Law (26), Amp (18), Chl (16), Phen (10), Arg (10), Apa (8), Qrz (6), Tnt (3), *Py, Hem*
10tav09	Tavşanlı Zone, Turkey	39°43′49.72″N; 29°49′19.93″E	Amp (28), Law (25), Chl (12), Phen (10), Arg (10), Apa (6), Qrz (4), Tnt (3), *Py, Hem*

Notes: Minerals in italic denote opaque accessory minerals identified in samples. Amp = amphibole; Chl = chlorite; Phen = phengite; Law = lawsonite; Tnt = titanite; Arg = aragonite; Cpx = clinopyroxene; Apa = apatite; Py = pyrite; Hem = hematite; Qrz = quartz; Mn-Grt = Mn-rich garnet; Ga = galena.

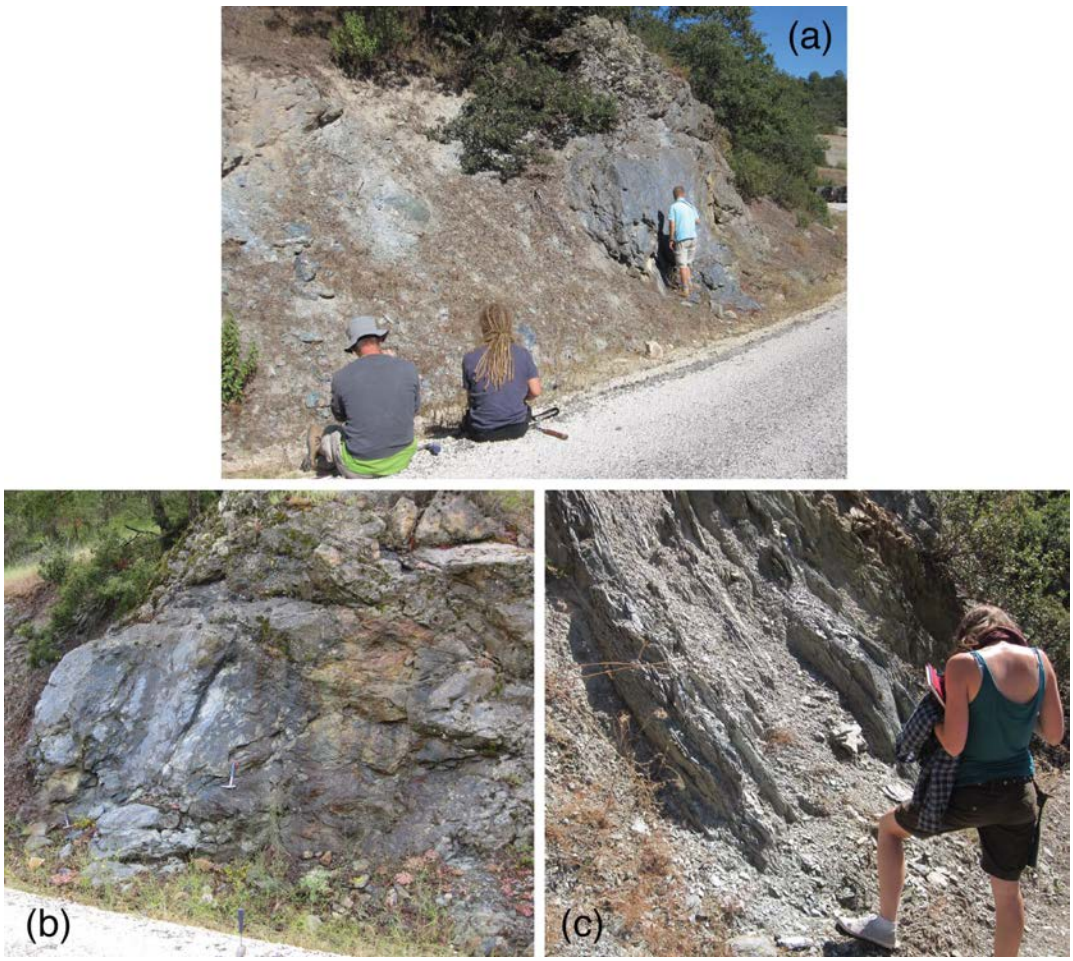

Figure 2. Field photographs: (**a**) Blueschist outcrops consist of a sequence of intercalated metabasite, metachert, metashale, and metagabbro blocks of different sizes in diameter, immersed in the mélange matrix; (**b**) location where blueschist samples 10tav04, 05, 07, and 09 were collected; (**c**) location where blueschist samples 10tav06 and 08 were collected. (Color online.)

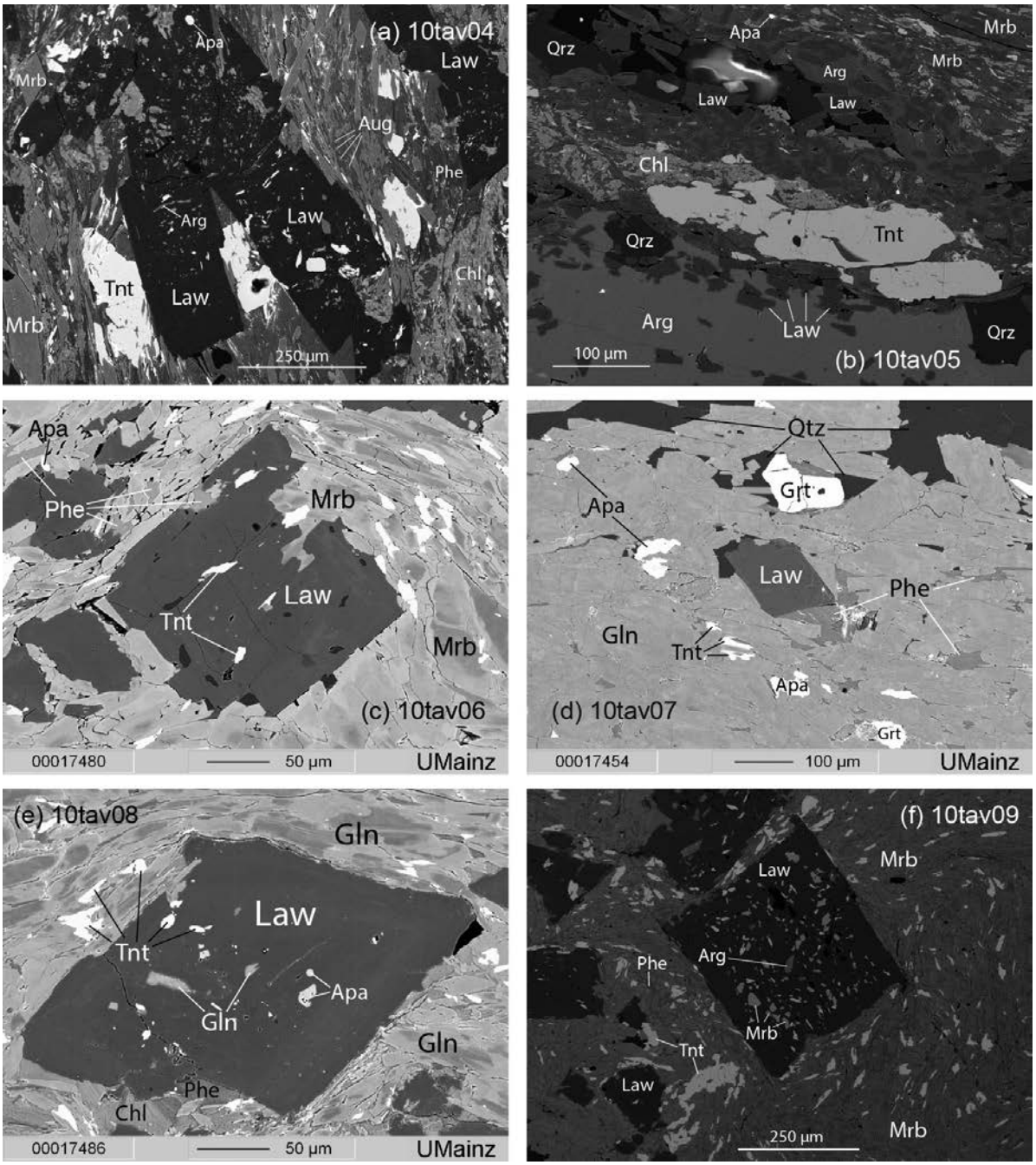

Figure 3. Representative backscattered electron images of Tavşanlı blueschists. (**a**) Sample 10tav04. Euhedral lawsonite filled with tiny sodic amphibole, augite, and titanite as inclusions along with interstitial anhedral aragonite. (**b**) Sample 10tav05. The only sample with highly carbonated foliation characterized by the preferred alignment of phengite, sodic amphibole, and to a lesser extent. Chlorite (**c**, **e**, and **f**) samples 10tav06, 08, and 09, respectively. These three samples share similar paragenesis of euhedral prismatic lawsonites coexisting with sodic amphibole, aragonite, phengite, chlorite, titanite, and apatite. (**d**) Sample 10tav07 shows the simplest texture and best-preserved idiomorphic mineral assemblage of all six samples and is the only sample where Mn-rich garnet occurs. Law = lawsonite; Gln = glaucophane; Mrb = magnesio-riebeckite; Tnt = titanite; Apa = apatite; Phe = phengite; Chl = chlorite; Aug = augite; Arg = aragonite; Grt = garnet; Qtz = quartz. (Color online.)

chlorite, titanite, apatite, aragonite, and accessory opaque pyrite and hematite. Euhedral lawsonite is prismatic and rhombic/rectangular, with up to 500 µm grains often filled with tiny sodic amphibole, augite, and titanite inclusions along with interstitial anhedral aragonite (Fig. 3a). Aragonite is recognized as the primary $CaCO_3$ polymorph by the lack of the perfect rhombohedral cleavage of calcite or dolomite and higher refractive indices. It is a characteristic mineral of HPLT metamorphism and

its occurrence in Tavşanlı zone blueschist has been reported in many previous publications where calcite pseudomorphs after aragonite were also identified (e.g., Okay 1980a, 1982; Davis and Whitney 2006; Çetinkaplan et al. 2008; Seaton et al. 2009; Whitney et al. 2014). Small (~20 μm) and relatively fine-grained igneous augite is found only in sample 10tav04, occurring as either single rectangular crystals or as aggregates of small prismatic grains (Fig. 3a); some previous work found it to be partially or completely replaced by sodic pyroxene (Okay 1980a, 1980b, 1982; Okay and Whitney 2010). It is normally overgrown by sodic amphibole at the periphery and along cleavages resulting in bleached, patchy crystals (Okay 1978, 1980a; Plunder et al. 2015). Sodic amphibole and phengite are intergrown with each other as acicular or elongated columnar crystals, and together with chlorite, they make up most of the groundmass. Titanite grain size varies from 5–100 μm, typically with sphenoidal shapes and intergrown almost everywhere, whereas apatite presents tiny subhedral rounded grains of ~5–15 μm.

10tav05. Sample 10tav05 exclusively exhibits large aragonite pools around lawsonite and quartz with a preferred alignment of phengite, sodic amphibole and, to a lesser extent, chlorite, which clearly differentiates it texturally from other samples (Fig. 3b). Quartz and apatite occur as porphyroblasts in an aragonite matrix together with much smaller euhedral rectangular lawsonite (10–100 μm). Chlorite and phengite are often entwined and aligned parallel to foliation with prismatic lawsonite, enclosing intergrowths of elongated sodic amphibole. Almost all lawsonite crystals in the matrix are idiomorphic and contain no inclusions other than tiny interstitial aragonite patches, implying that carbonation might have taken place entirely prior to lawsonite growth during formation of the foliation. Titanite grain size varies greatly (5–50 μm) and always occurs in crevices as late fillings between different minerals. Apatite is generally included in the aragonite matrix with larger grain size of up to 100 μm. Galena appears only in sample 10tav05 as the accessory sulfide mineral instead of pyrite.

10tav07. Sample 10tav07 has the simplest texture and best preserved idiomorphic mineral assemblage. Lawsonite shows ubiquitous euhedral rhombic or square grains 50–800 μm in size, and it only rarely comprises interstitial titanite, quartz, and sodic amphibole inclusions (Fig. 3d). Quartz forms a coarse-grained matrix together with sodic amphibole. Euhedral/subhedral garnets appear only in this sample and are enriched in manganese with occasional titanite or sodic amphibole inclusions of variable size (10–250 μm). Sodic amphibole mostly occurs as single tabular and acicular crystals or lath-like aggregates intergrown with phengite and chlorite. Phengite is also found between quartz and lawsonite grains or enclosing lawsonite. Large titanites (average size ~100 μm) occur throughout the sample, whereas apatite may occur as inclusions in titanite and generally appears as anhedral fine-grained crystals. No sign of carbonation or other later stage alteration is observed in this sample, implying well-preserved initial metamorphism.

10tav06, 10tav08, and 10tav09. These three samples share similar parageneses and textures (Figs. 3c, 3e, and 3f), with a mineral assemblage of lawsonite, sodic amphibole, quartz, aragonite, phengite, chlorite, titanite, apatite, and opaque accessory minerals (pyrite and hematite). Euhedral prismatic lawsonites occur in all three samples as porphyroblasts with variable grain size (50–1000 μm), and usually with interstitial quartz, aragonite, sodic amphibole, and titanite crystals as inclusions, exhibiting a patchy surface with sodic amphibole, phengite, and chlorite. Aragonite and quartz occur mostly as tiny inclusions embedded in lawsonite grains, whereas sodic amphibole, chlorite, and phengite appear almost everywhere intergrown together as an acicular or columnar shape with subhedral titanite and apatite crystals inserted in crevices. Calcic amphibole (actinolite) replaces some of the sodic amphibole (glaucophane) at the rim in sample 10tav08, indicating a small degree of retrograde metamorphism, and occasional oscillatory zoning of lawsonite can be seen only in this sample.

Whole-rock geochemistry

The major and trace element compositions of the six samples are listed in Table 2.

Major elements. Samples 10tav06, 08, and 09 have similar major element compositions, implying analogous protoliths. Specifically, they show mafic compositions with consistent SiO_2 contents of 44.8–46.5 wt%, FeO_T 11.1–11.2 wt%, CaO 10–12.2 wt%, Na_2O 2.3–2.8 wt%, and almost identical TiO_2, MnO, K_2O contents of 1.4, 0.16, and 0.1 wt%, respectively. Sample 10tav06 has slightly lower Al_2O_3 (14 wt%) and higher MgO (7 wt%) than the other two (15.3–15.5 and 4.7–5.6 wt%), whereas 10tav09 exhibits the lowest Mg number of 42.8. All show similar LOI of approximately 7.5, higher than the typical value of unaltered lawsonite blueschist containing phengite, indicating slight late alteration.

Samples 10tav04 and 05 are mafic with SiO_2 around 45 wt%, whereas sample 10tav07 has higher SiO_2 (57.5 wt%), reflecting its high quartz content. Sample 10tav04 is the most K-, Na-, Ti- and Fe-rich rock with 2.9, 3.8, 1.5 and 13.3 wt%, respectively, and contains the lowest CaO (5.3 wt%). The high K content results from large and abundant phengite grains, indicating a continental sedimentary origin for the blueschist protolith, whereas the Ca depletion is consistent with the lowest lawsonite content in these rocks. Sample 10tav05 has the highest volatile contents (10% LOI) due to its carbonate alteration, whereas sample 10tav07 has the lowest LOI value of 3.9%, marking its well-preserved unaltered nature.

For all six samples, MgO varies little (4.7–7.1 wt%), slightly lower than mid-ocean ridge basalt (MORB) and higher than global subducted sediment (GLOSS) (Fig. 4), and they present low Mg numbers of 42.8–54.9. Samples 10tav06, 08, and 09 show compositions compatible with MORB for major elements, whereas samples 10tav04, 05, and 07 are not compatible with MORB for the majority of major elements (Fig. 4). Contents of Al_2O_3, CaO, and K_2O, particularly K_2O indicate GLOSS-like affinities, i.e., continent-derived terrigenous sediment (Figs. 4b, 4d, and 4f). The enrichment of K and depletion of Ca in Franciscan blueschists was also attributed to the presence of terrigenous sediment in the source (Sorensen et al. 1997; Ukar 2012; Ukar and Cloos 2015).

Trace elements. Samples 10tav06, 08, and 09 show similar N-MORB-like trace element affinities (Fig. 5), exhibiting only slight Th and U enrichments and similar Nb, Ta, and REE concentrations to N-MORB (Fig. 5). Although slightly enriched in

TABLE 2. Major (wt%) and trace (ppm) element compositions of blueschists

Sample	10tav04	10tav05	10tav06	10tav07	10tav08	10tav09
No. of anal.	5	5	5	5	5	5
SiO_2	47.6	43.8	45.4	57.5	46.5	44.8
TiO_2	1.5	0.9	1.4	1.2	1.4	1.4
Al_2O_3	13.9	14.9	13.9	12.9	15.5	15.3
FeO_T	13.3	9.3	11.2	8.2	11.1	11.2
MnO	0.19	0.21	0.18	0.15	0.15	0.16
MgO	7.1	6.3	7.0	5.6	5.4	4.7
CaO	5.3	11.9	11.2	6.0	10.0	12.2
Na_2O	3.8	2.1	2.7	3.1	2.3	2.8
K_2O	2.9	0.7	0.1	0.9	0.1	0.1
P_2O_5	0.2	0.1	0.1	0.2	0.1	0.1
Cr_2O_3	0.02	0.07	0.04	0.03	0.04	0.05
NiO	0.01	0.02	0.02	0.02	0.01	0.01
LOI	4.0	10.0	7.2	3.9	8.0	7.6
Sum	99.9	100.2	100.4	99.7	100.4	100.3
Li	27	25	22	27	33	37
Sc	45	40	42	27	43	35
Ti	10287	6399	9999	10364	10872	6770
V	372	235	248	205	287	227
Cr	145	512	270	254	309	210
Mn	1360	1620	1346	1233	1303	845
Co	42	51	39	28	49	35
Ga	18	14	15	17	18	13
Rb	75	17	2.6	22	2.1	2.1
Sr	42	343	185	144	84	71
Y	35	24	28	37	34	26
Zr	80	58	75	212	97	65
Nb	5.9	20	5.1	32	4.5	2.8
Cs	3.2	0.68	0.14	0.5	0.11	0.16
Ba	297	56	11	144	5.3	17
La	6.2	15	4.4	36	5.2	6.8
Ce	15	26	11	69	13	11
Pr	2.3	3.0	1.7	8.5	2.1	2.2
Nd	12	13	9.4	35	11	10
Sm	4.0	3.0	3.3	7.8	3.7	3.1
Eu	1.4	1.1	1.1	2.1	1.4	1.1
Gd	5.4	3.7	4.0	7.5	5.0	3.7
Tb	0.95	0.60	0.74	1.1	0.91	0.66
Dy	6.6	4.1	5.0	7.0	6.2	4.4
Ho	1.4	0.91	1.1	1.4	1.4	0.94
Er	3.9	2.7	3.1	3.9	3.9	2.7
Tm	0.53	0.38	0.47	0.55	0.53	0.39
Yb	3.5	2.6	3.3	3.6	3.7	2.6
Lu	0.47	0.38	0.46	0.52	0.53	0.40
Hf	2.3	1.6	2.2	5.1	2.7	1.8
Ta	0.32	1.1	0.31	2.0	0.27	0.15
Pb	1.8	10	2.0	2.4	5.7	10
Th	0.36	1.9	0.36	7.9	0.38	0.24
U	0.27	0.37	0.18	1.6	0.26	0.33
Ba/Th	825	29	31	18	14	71
Ce/Nb	2.5	1.3	2.2	2.2	2.9	3.9
La/Sm	1.6	5.0	1.3	4.6	1.4	2.2
Rb/Sr	1.8	0.05	0.01	0.15	0.03	0.03
Ba/Rb	4.0	3.3	4.2	6.5	2.5	8.1
Nb/La	0.95	1.3	1.2	0.89	0.87	0.41
Th/Yb	0.10	0.73	0.11	2.2	0.10	0.09
La/Yb	1.8	5.8	1.3	10	1.4	2.6
Ta/Yb	0.09	0.42	0.09	0.56	0.07	0.06
Ce/Pb	8.3	2.6	5.5	29	2.3	1.1
Nb/U	22	54	28	20	17	8.5
Th/Nb	0.06	0.10	0.07	0.25	0.08	0.09

Cs, Rb, and Ba relative to N-MORB, these three samples still exhibit significantly lower large-ion lithophile element (LILE) concentrations than GLOSS. In contrast, samples 10tav04, 05, and 07 are substantially enriched in LILE, such as Cs, Rb, and Ba 10–1000× N-MORB, except for insignificant/negative Sr anomalies (Fig. 5). Moreover, they have more enriched LILE, Th, U, Nb, Ta, and higher light rare earth elements (LREE) similar to GLOSS, particularly for sample 10tav07 (Fig. 5), which clearly distinguishes them from samples 10tav06, 08, and 09. Sample 10tav04 has a notably elevated Ba/Th ratio (825). All six samples are enriched in Pb and Li relative to N-MORB (Fig. 5), and all exhibit variable contents of Ni, Cr, and V (Ni = 70–199 ppm, Cr = 145–512 ppm; V = 205–372 ppm).

Mineral chemistry

Major and trace element compositions of all minerals are listed in Supplemental[1] Tables S1 and S2, and Appendices S1–S7. For lawsonite and titanite, iron was assumed to be Fe^{3+}, whereas Fe^{2+} was used for phengite, garnet, and chlorite. Fe^{2+} and Fe^{3+} abundances in amphibole were calculated by charge balance (Supplemental[1] file S2; Schumacher 1997).

Lawsonite. The major element compositions of lawsonite are consistent in all six samples and denote an almost ideal structural formula of $CaAl_2Si_2O_7(OH)_2(H_2O)$. They have ~1.1–1.7 wt% Fe^{3+} and almost negligible Cr and Ti except for sample 10tav08 (0.13 wt% Cr_2O_3, Supplemental[1] Table S3) where oscillatory zoning is observed, in good agreement with previous studies (e.g., Sherlock et al. 1999). Lawsonites in all samples show a negative correlation between Si and Al + Ca (atomic) (Supplemental[1] Fig. S1).

Despite the restricted major element compositional variation, lawsonites exhibit extremely complex and heterogeneous trace element compositions. Numerous studies have affirmed that lawsonite is a significant repository for Sr, Pb, Th, U, and REE (e.g., Tribuzio et al. 1996; Ueno 1999; Spandler et al. 2003; Vitale Brovarone et al. 2014; Martin et al. 2014), because the structure of lawsonite allows divalent elements (e.g., Sr and Pb) to enter the Ca site and trivalent REE to be charge balanced by M^{2+} on the octahedral site. Samples 10tav04 and 10tav07 show the highest REE concentrations with nearly flat REE patterns. Sample 10tav05 exhibits relatively enriched LREE contents (Fig. 6). LILE (Cs, Rb, and Ba) are slightly depleted in all lawsonites, whereas HFSE are similar to or slightly higher than chondrite. Th and U are remarkably enriched in sample 10tav07 with over 2 orders of magnitude higher than in other samples.

Another noteworthy feature in lawsonite is its compositional heterogeneity (e.g., Ueno 1999; Vitale Brovarone et al. 2014; Martin et al. 2014; Dubacq and Plunder 2018) reflected in large standard deviations in Figure 6. Using X-ray and Confocal MicroRaman 3D spectroscopic mapping results (Supplemental[1] Fig. S2), we can exclude the possibility that this is due to the presence of inclusions and/or impurities, because only tiny quartz, sodic amphibole, and titanite grains are identified, none of which has significant abundances of Th, U, and REE that could falsify the lawsonite compositions. In addition, we also exclude zoning as the cause of the compositional heterogeneity because except for sample 10tav08, no marked zoning is observed for the lawsonites.

Amphibole. Amphiboles are mostly sodic (6.5–10.4 wt% Na_2O) except in sample 10tav08, which also shows calcic compositions (Supplemental[1] Material S2; Supplemental[1] Fig. S3). Chemically, sodic amphiboles vary from glaucophane to Fe-rich glaucophane/magnesio-riebeckite. All glaucophanes show consistent compositions with ~57 wt% SiO_2, 10 wt% MgO, 10 wt% Al_2O_3, and 12 wt% FeO_T, whereas magnesio-riebeckites have similar SiO_2 and MgO contents but lower Al_2O_3 (~4.5 wt%) and higher FeO_T (~18 wt%). Actinolite in sample 10tav08 has the highest MgO and CaO and the lowest Na_2O content (1.6 wt%). Winchite in sample 10tav05 is higher in sodium and iron.

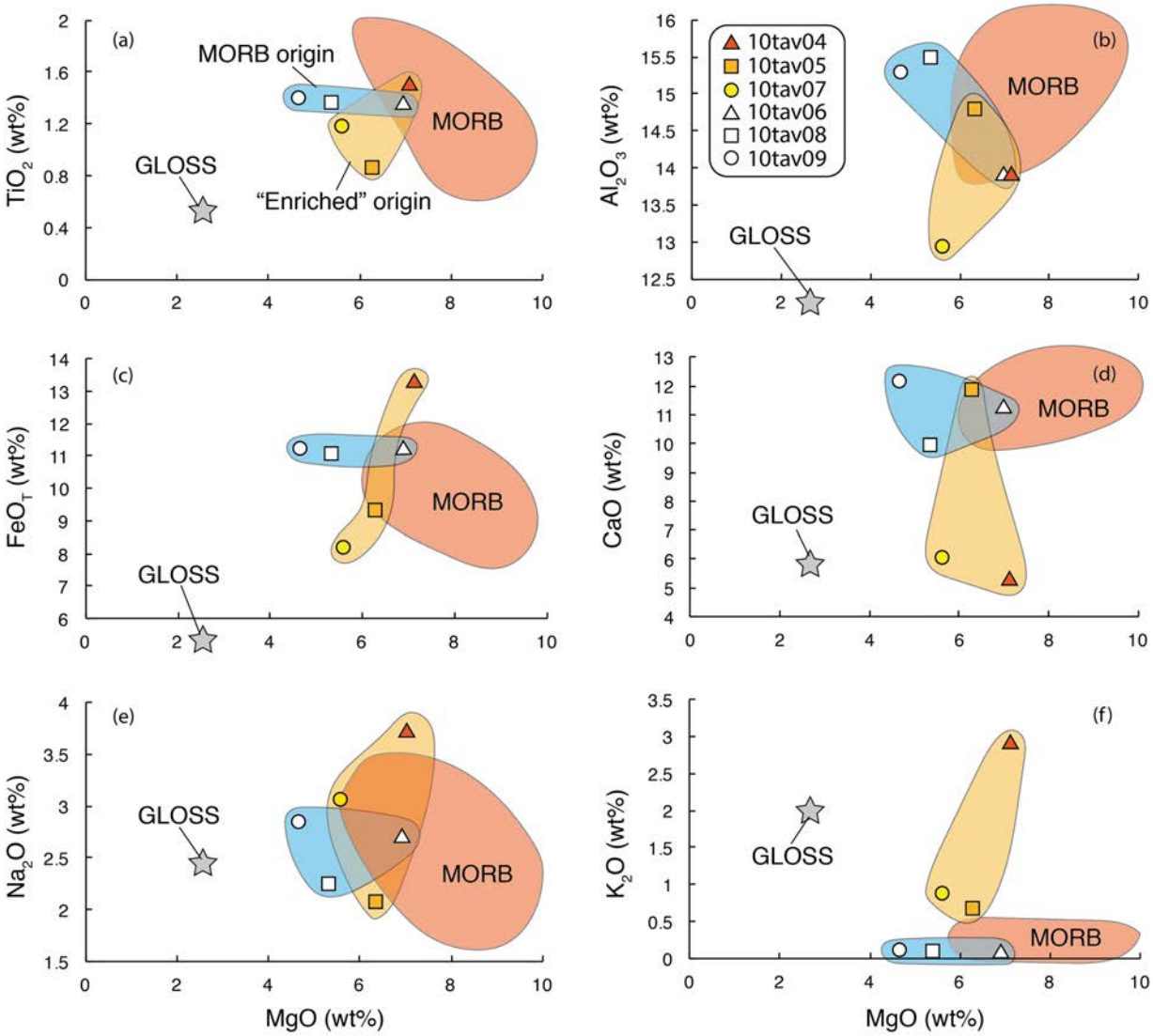

FIGURE 4. MgO variation diagrams of six key major elements (Ti, Al, Fe, Ca, Na, and K from **a** to **f**, respectively) in the Tavşanlı zone blueschists. Also shown are MORB compositions (orange shaded fields, GEOROC database, http://georoc.mpch-mainz.gwdg.de/georoc) and GLOSS (gray stars, Plank and Langmuir 1998). Blue shaded "MORB origin" fields include samples 10tav06, 08, and 09, whereas yellow shaded "enriched origin" fields include samples 10tav04, 05, and 07. (Color online.)

All amphiboles exhibit consistently flat REE patterns above unity except for glaucophane in 10tav07, which has REE below C1 chondrite (Fig. 7a). Samples 10tav04, 06, and 08 are enriched in Cs, Rb, and Ba, possibly because of the presence of retrograde amphiboles (sample 10tav08) or slight contamination by phengite during analysis (Fig. 7a). Winchite in sample 10tav05 exhibits the most Th, U, Nb, Ta, and LREE enrichment, whereas glaucophanes in samples 10tav07 and 09 show the most depleted Rb, Ba, Nb, and Ta. In Supplemental[1] Fig. S4, clear distinctions between amphibole types can be seen; calcic amphiboles carry the most Cs, Rb, and Ba while glaucophanes and riebeckites host the least, and winchite carries the most Sr.

Phengite. Mica formulas were calculated using 22 oxygen atoms, and all exhibit high Si contents of up to 7.3 atoms per formula unit (apfu) and extremely low Na content of ~0.01 apfu indicating no paragonite component (Appendix[1] S1). Potassium is approximately 10.5 wt% K_2O in all samples, whereas MgO content varies from 5.1 to 7.1 wt%. Phengites host considerable LILE (except for Sr) with 2–3 orders of magnitude higher than C1 chondrite (Fig. 7c). Limited by the fine and elongated crystal size, we could only measure phengites in two samples, but these should be representative for all samples since the results are in good agreement with each other and with previous studies (Xiao et al. 2014; Martin et al. 2014). In sample 10tav07, some selected trace element compositions (especially HFSEs such as Th, U, Nb, Ta, and HREE) are conspicuously higher than in 10tav04, which exhibits a flat pattern slightly above unity; we interpret this as possible slight lawsonite (Th, U, and HREE) or titanite (Nb, Ta) contamination. However, Cs, Rb, and Ba will remain unaffected by any titanite contamination, so that the

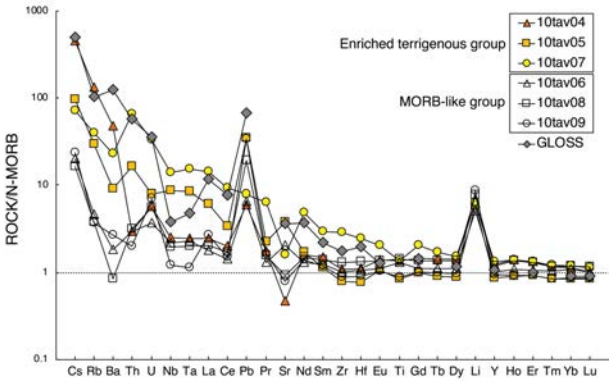

FIGURE 5. Whole-rock trace element compositions of blueschist samples from the Tavşanlı zone along with Global Subducted Sediments (GLOSS, Plank and Langmuir 1998), normalized to N-MORB (Sun and McDonough 1989). (Color online.)

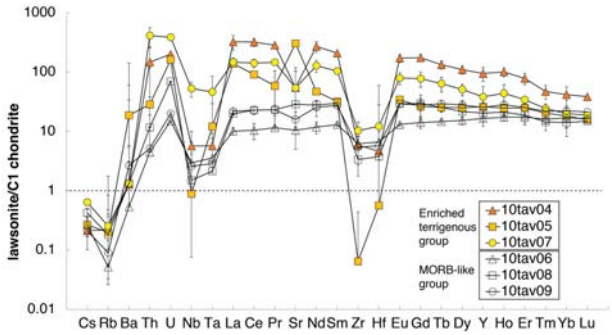

FIGURE 6. Trace element compositions of lawsonite in the Tavşanlı zone blueschists, normalized to C1 chondrite (Sun and McDonough 1989). Error bars indicate propagated uncertainties as single standard deviations. (Color online.)

differences between samples 10tav04 and 07 in Supplemental[1] Fig. S5 are attributable to phengite itself. Sample 10tav07 has higher Ba, Sr, and Rb than that of sample 10tav04, whereas Cs is more enriched in sample 10tav04.

Chlorite. In sample 10tav07, chlorites show the highest Si and Mg contents (6.56 and 6.85 apfu), and lowest Al and Fe, suggesting diabantite composition, whereas the other samples present typical chlorite formula of $(Mg,Fe)_3(Si,Al)_4O_{10}(OH)_2\cdot(Mg,Fe)_3(OH)_6$ with only slight compositional differences (~28 wt% SiO_2, 17 wt% Al_2O_3 and 21 wt% MgO). Chlorites yield the lowest trace element concentrations of all minerals except in sample 10tav04, which shows moderate Cs, Rb, and Ba enrichments and slightly higher REE concentrations (Fig. 7e).

Titanite and apatite. There is little major element variation in titanite and apatite, both close to the standard structural formulas of $CaTi(SiO_4)(O,OH,F)$ and $Ca_5(PO_4)(OH,F,Cl)$. In contrast, there are strong distinctions in the trace element compositions of titanite grains. Titanites in all samples (particularly 10tav05 and 07) contain the highest Nb and Ta of all minerals (up to 723 and 41 ppm, respectively) and relatively high Th, U, and REE (Fig. 7b). In sample 10tav05, REE appears to have a slightly downward sloping pattern (HREE-depleted), whereas the rest of samples give uniformly upward arrays (LREE-depleted), most marked in sample 10tav06 with considerably lower concentrations. Spandler et al. (2003) attributed these chemical differences to the different timing of titanite growth with respect to other trace element-rich minerals, and to variations in whole-rock trace element contents. The upward sloping REE patterns in our samples probably formed from an LREE-depleted matrix after lawsonite crystallization and in the presence of zircon (indicated by the relatively low Zr and Hf contents), whereas the downward sloping REE pattern of 10tav05 can be interpreted as crystallizing prior to lawsonite because LREE would have been taken up in lawsonite otherwise. Apatite is widely acknowledged as an important host of Sr, Pb, and REE (e.g., Haggerty et al. 1994; Martin et al. 2014): in this study it yields moderately enriched REE with slight preference of HREE over LREE in most samples, and all apatites exhibit strong Sr affinity (Fig. 7d).

Other minerals. Garnet (~1 mode%) is found only in sample 10tav07 characterized by decreasing spessartine from core to rim (41 to 25%). This distinctive occurrence of a minute amount of Mn-rich garnet is probably due to multiple factors, including the breakdown of hydrous minerals (e.g., chlorite, amphibole, lawsonite, and phengite), the composition of parental rocks and the PT conditions of metamorphic reactions (Xia and Zhou 2017). Piemontite and Mn-rich garnet are also reported from quartz-rich schists elsewhere in the Tavşanlı zone (Okay 1980; Davis and Whitney 2006). In agreement with previous findings (e.g., Hauri et al. 1994; Van Westrenen et al. 2001), garnet shows an extremely strong preference for HREE over LREE with up to ~3 orders of magnitude higher than C1 chondrite (Fig. 7f). Moreover, garnet hosts considerable Th and U, which is uncommon because they would usually not be expected to enter garnet, particularly in the presence of lawsonite (Spandler et al. 2003; Martin et al. 2014). We suggest this might be due to either the effect of the manganese-rich composition on the garnet structure or possibly minor contamination from other minerals such as titanite or lawsonite. Aragonite is the only carbonate phase and carries significant amounts of Ba and Sr (Fig. 7f). Galena is only seen in sample 10tav05, whereas hematite and pyrite are found in all samples. Hematite unexpectedly hosts significant amounts of Ba, Th, U, and REE with strong LREE affinity over HREE of ~3 orders of magnitude higher than C1 chondrite (Fig. 7f).

Isotope constraints

This study provides the first Sr-Nd-Pb isotopic constraints of the Tavşanlı zone blueschists (Supplemental[1] Tables S3 and S4). Whole-rock Sr, Nd, and Pb isotopic results together with incompatible trace element concentrations indicate considerable differences in the extent of trace element enrichment among the samples, which lead over time to a wide variety of isotopic signatures in blueschists (Figs. 8 and 9).

Samples 10tav06, 08, and 09 have low concentrations of K, Th, U, and REE, plotting in a restricted area on the Sr-Nd isotopic diagram (Fig. 8), with unradiogenic $^{87}Sr/^{86}Sr$ (0.7052–0.7057) and radiogenic $^{143}Nd/^{144}Nd$ (~0.5129) similar to MORB. Samples 10tav06 and 08 also have the most unradiogenic $^{206}Pb/^{204}Pb$

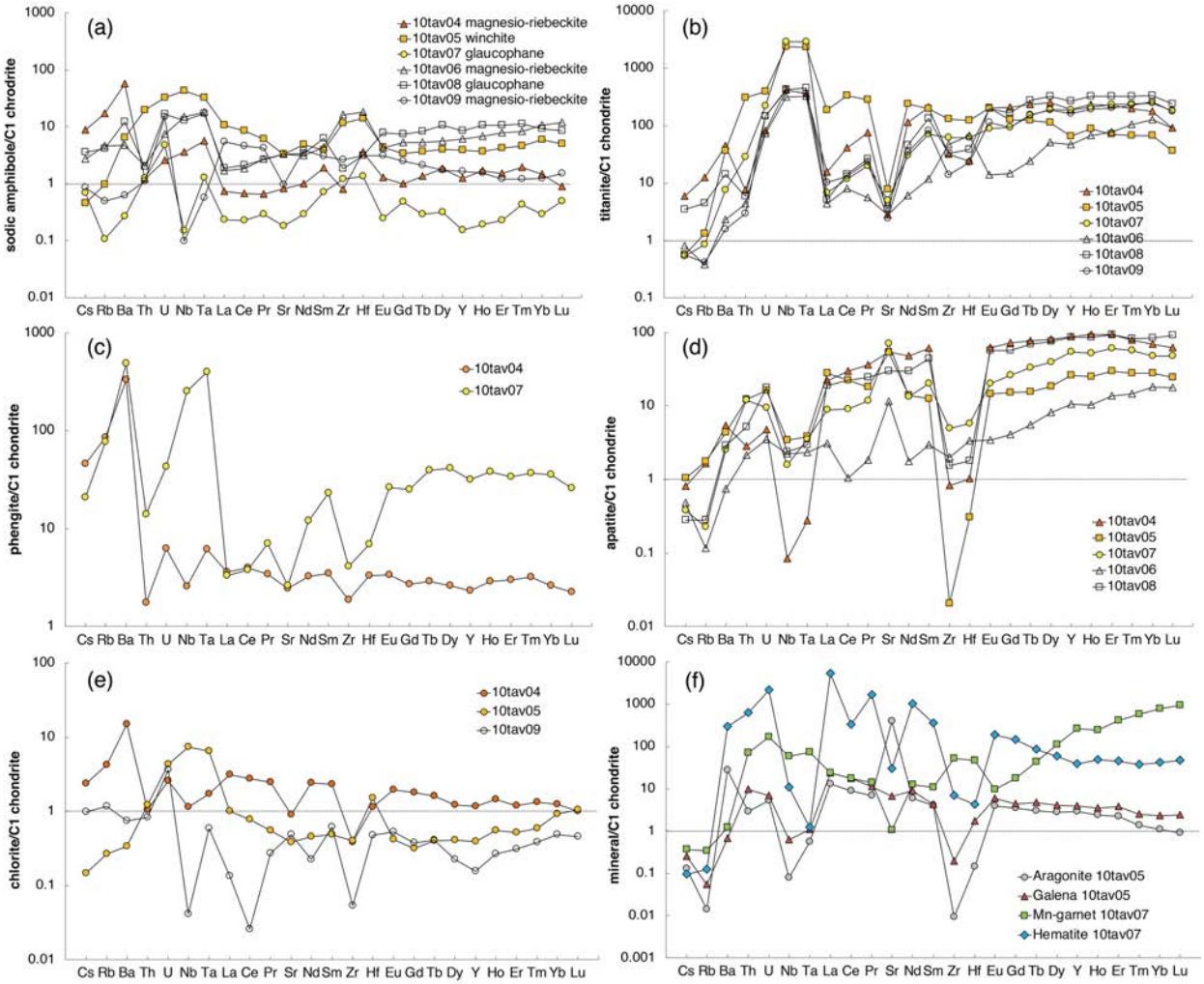

FIGURE 7. Pb isotopic variation of the Tavşanlı zone blueschists (modified from Prelević et al. 2015). (**a**) $^{206}Pb/^{204}Pb$ vs. $^{207}Pb/^{204}Pb$ and (**b**) $^{206}Pb/^{204}Pb$ vs. $^{208}Pb/^{204}Pb$. NHRL = Northern Hemisphere Reference Line from Hart (1984). (Color online.)

(18.33–18.42), $^{207}Pb/^{204}Pb$ (15.57–15.60), and $^{208}Pb/^{204}Pb$ (38.37–38.47) compositions (Fig. 9), plotting broadly within the depleted MORB mantle (DMM) field, consistent with a MORB-like oceanic crust protolith. Samples 10tav04, 05, and 07, which are more enriched in K, Th, U, and LREE, have variably radiogenic $^{87}Sr/^{86}Sr$ and mostly unradiogenic $^{143}Nd/^{144}Nd$. Sample 10tav04 has similar radiogenic $^{143}Nd/^{144}Nd$ (~0.5129) to samples 10tav06, 08, and 09 but much more radiogenic $^{87}Sr/^{86}Sr$ (up to 0.7070) compositions (Fig. 8), whereas its Pb isotopes are slightly higher than 10tav06 and 08 (Fig. 9), implying an enriched protolith and addition of slab-derived Sr-rich fluid. Sample 10tav07 has the most unradiogenic $^{87}Sr/^{86}Sr$ (~0.7053) and $^{143}Nd/^{144}Nd$ (0.5125) as well as the most radiogenic $^{206}Pb/^{204}Pb$ (19.35), $^{207}Pb/^{204}Pb$ (15.66), and $^{208}Pb/^{204}Pb$ (39.74) compositions, implying the presence of some enriched, probably continental crust-like, component. Samples 10tav04 and 07 show more radiogenic $^{206}Pb/^{204}Pb$, $^{207}Pb/^{204}Pb$, and $^{208}Pb/^{204}Pb$ isotopic compositions relative to 10tav06 and 08, although they mostly plot close to the Northern Hemisphere Reference Line (NHRL; Hart 1984; Fig. 9).

DISCUSSION

Blueschists with two different protolith lithologies

Possible protolith lithologies of blueschists. Constraining blueschist protoliths can reveal several key pieces of information concerning the tectonic evolution and related volcano-sedimentary processes at subduction zones (Ernst 1988; Stern 2005; Palin and White 2015). Protolith lithologies of mafic blueschists in oceanic subduction zones are widely acknowledged to be derived from the upper part of the oceanic crust consisting of a thin veneer of sediments, segments of igneous rocks, and depleted peridotite (Karson 2002; Klemd 2013). Specifically, the protoliths of mafic blueschist could be normal or enriched mid-ocean ridge basalt (N-/E-MORB; e.g., Honegger et al. 1989; Becker et al. 2000; Song et al. 2009; Zheng et al. 2010; Ukar et al. 2015), ocean island basalt (OIB; e.g., Volkova and Budanov 1999; Tang and Zhang 2013; Ge et al. 2016), and sometimes both MORB and OIB (e.g., Patočka and Pin 2005; Maulana et al. 2013). In addition, some blueschists could be derived from

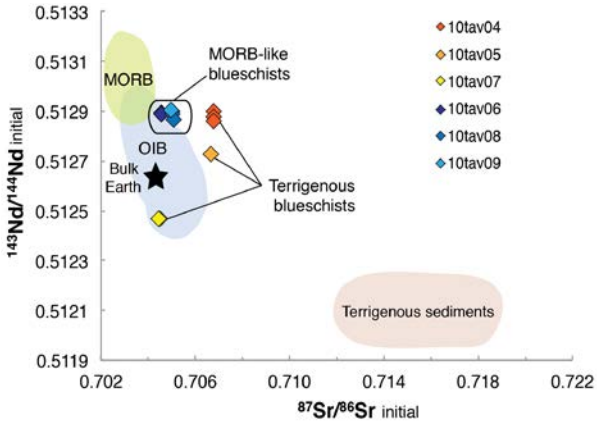

FIGURE 8. $^{87}Sr/^{86}Sr$ and $^{143}Nd/^{144}Nd$ isotopic variation (initial values) of lawsonite blueschists. Sr and Nd isotopic data for MORB and OIB from the GEOROC database (http://georoc.mpch-mainz.gwdg.de/georoc), terrigenous sediment field from Rollinson (2014). (Color online.)

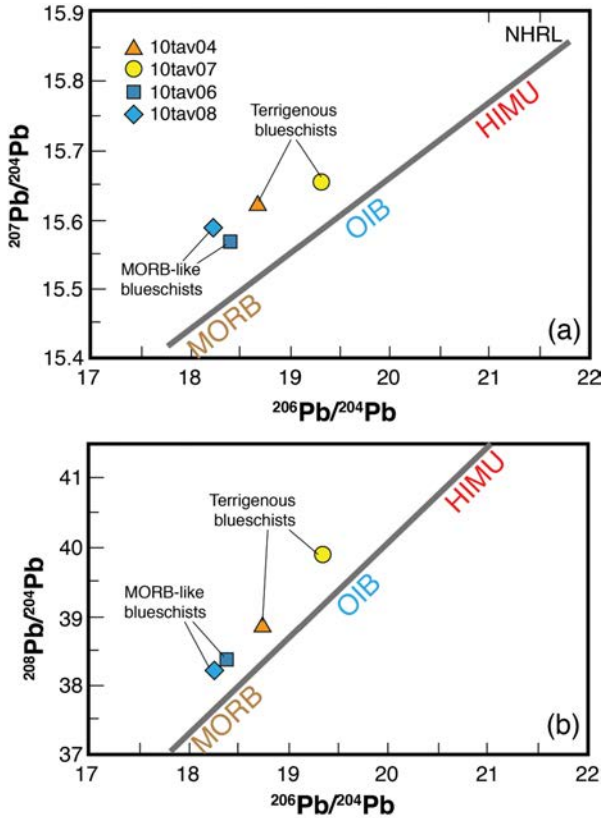

FIGURE 9. Pb isotopic variation of the Tavşanlı zone blueschists (modified from Prelević et al. 2015). (**a**) $^{206}Pb/^{204}Pb$ vs. $^{207}Pb/^{204}Pb$ and (**b**) $^{206}Pb/^{204}Pb$ vs. $^{208}Pb/^{204}Pb$. NHRL = Northern Hemisphere Reference Line from Hart (1984). (Color online.)

an ophiolitic complex (e.g., Volkova et al. 2009; Zhang et al. 2009), or volcanoclastic rocks (e.g., Miller et al. 2009). Clear enriched affinities have also been identified in protoliths of mafic blueschists: some have been attributed to the involvement of sediments in the source (e.g., Bernard-Griffiths et al. 1986; Ukar 2012), whereas Zhu et al. (2015) proposed that they originated from a continental rift environment. Furthermore, dehydration at high pressures may induce metasomatism that could exert a strong effect on blueschist compositions, and these metasomatizing fluids would dramatically reshape the trace element compositions by fluid-rock interaction (e.g., Beinlich et al. 2010; Klemd 2013; Vitale Brovarone et al. 2014; Kleine et al. 2014).

Only a few petrological and geochemical studies of the Tavşanlı zone blueschists have focused on the protoliths. The general consensus is that they are derived from volcano-sedimentary sequences, whereas the mafic blueschists in this study were often interpreted as former basaltic rocks (e.g., Okay 1980, 1982; Çetinkaplan et al. 2008; Okay and Whitney 2010). Davis and Whitney (2006) proposed that these blueschists have an NMORB-like protolith that experienced seafloor metamorphism or fluid infiltration during subduction but prior to HP-LT metamorphism; Özbey et al. (2013) argued that they originated from both OIB and MORB sources, possibly affected by crustal contamination and variable amounts of fractional crystallization. However, more diagnostic geochemical proxies, especially isotopic compositions, are required to further constrain the protoliths of mafic blueschists in the Tavşanlı zone.

Two groups of blueschists in this study. Based on the whole-rock major and trace element geochemistry, mineral parageneses, and isotopic affinities, we divide our samples into two groups, namely MORB-like blueschist and enriched terrigenous blueschist. The first group includes samples 10tav06, 08, and 09, and is characterized by low concentrations of LILE (K, Cs, Rb, and Ba), HFSE (Th, U, Nb, Ta, and REE), coupled with variably unradiogenic $^{87}Sr/^{86}Sr$ and radiogenic $^{143}Nd/^{144}Nd$ compositions similar to MORB (Figs. 5 and 8). The second group includes samples 10tav04, 05, and 07 and differs from the first group in having LILE (up to 2.9% K_2O), HFSE (e.g., Th up to 7.8 ppm), and REE contents considerably higher than MORB, together with more radiogenic $^{87}Sr/^{86}Sr$ and unradiogenic $^{143}Nd/^{144}Nd$ isotopic compositions (particularly 10tav07, Figs. 5 and 8), consistent with an enriched continental sedimentary source.

Since the contents of fluid-mobile elements such as K, Na, Rb, Ba, Cs, Rb, La, and Ce are subject to later stage processes, while elements such as high field strength element (HFSE), REEs (except for La and Ce), Ni, V, and Cr should survive these relatively unchanged, the latter are often utilized to identify magmatic affinity (Rollinson 1993). Here we use Ti, Zr, and Nb to interpret the original tectonic settings of the magmatism as these elements should be little modified in blueschist metamorphism (Pearce and Cann 1973; Pearce 1975; Winchester and Floyd 1976; Wood 1980; Ukar and Cloos 2015). All blueschists but one plot in the tholeiitic field, although 10tav04 falls very close to the border between alkaline and tholeiitic in Figure 10a. Their tholeiitic nature is more pronounced in the P_2O_5 vs. Zr (Fig. 10b) and V vs. Ti plots (Supplemental[1] Fig. S5). In the Th/Yb vs. Ta/Yb diagram, samples 10tav06, 08, and 09 are clearly MORB-like, whereas 10tav05 and 07 plot toward the enriched end, which we attribute to continental crustal material (Fig. 10c). Thorium is much more sensitive to continental crust involvement than Ta, whereas Yb usually remains relatively stable in diverse enrichment processes (Pearce 1983). Sample

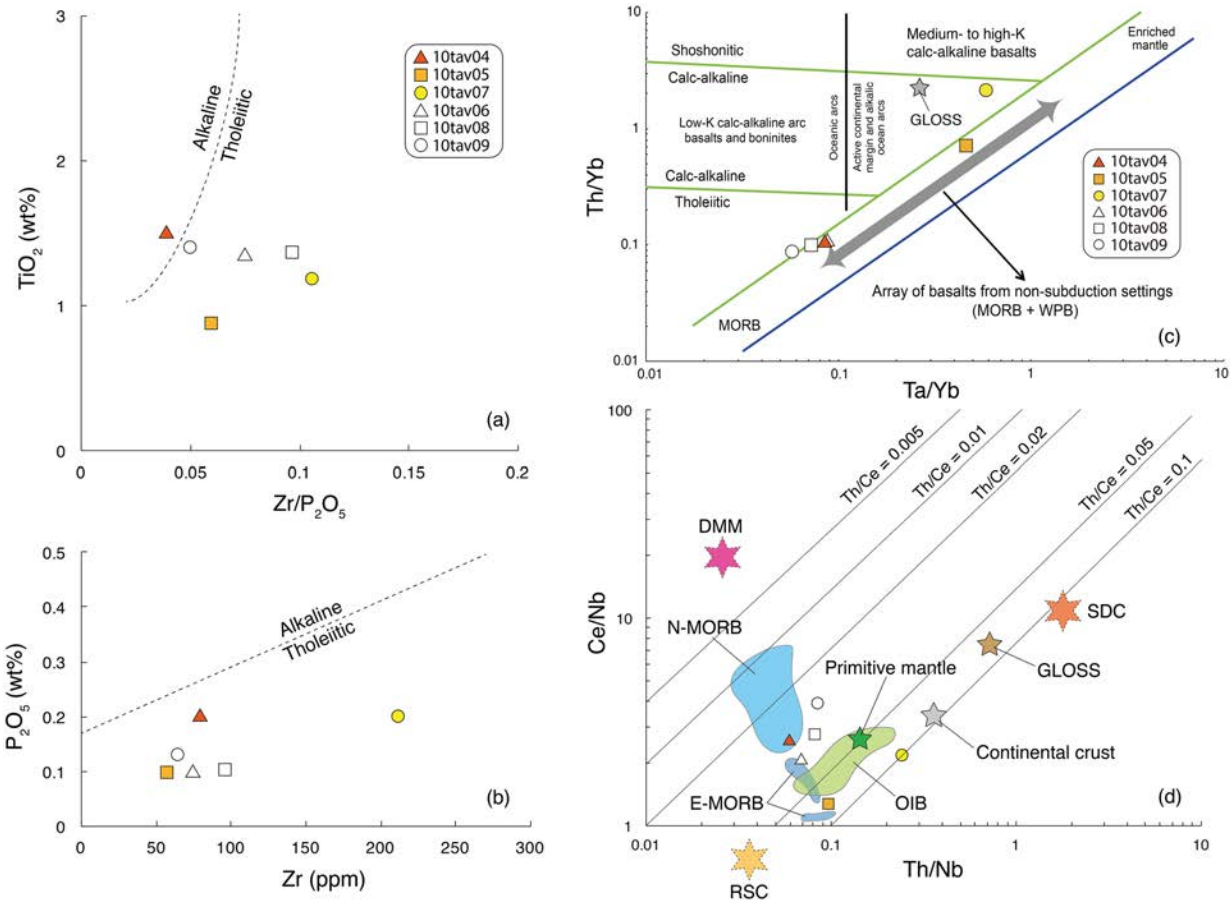

FIGURE 10. Discrimination diagrams: (**a**) TiO_2 vs. Zr/P_2O_5. Most blueschist samples are of tholeiitic affinity, except for sample 10tav04 that falls close to the line between alkaline and tholeiitic (after Winchester and Floyd 1976); (**b**) P_2O_5 vs. Zr (ppm) (after Winchester and Floyd 1976). All blueschists plot within the tholeiitic field; (**c**) Th/Yb vs. Ta/Yb discrimination diagram after Pearce (1983); (**d**) Ce/Nb vs. Th/Nb discrimination diagram following Saunders et al. (1988). DMM = Depleted MORB Mantle; RSC = Residual Slab Component; SDC = Slab-Derived Component; GLOSS = Global Subducted Sediments. (Color online.)

10tav04, however, plots together with MORB-like blueschists and does not show a pronounced continental crust affinity (Fig. 10c). A similar situation is seen in Ce/Nb vs. Th/Nb where samples 10tav05 and 07 plot well outside the N-MORB field and samples 10tav04, 06, 08, and 09 all fall near the N-MORB area (Fig. 10d), implying two different mantle sources for the oceanic basalts. Samples 10tav04, 06, 08, and 09 are of regular MORB origin, whereas samples 10tav05 and especially 07, are clearly affected by a continental crust component, probably terrigenous sediments similar to GLOSS (Saunders et al. 1988; Plank and Langmuir 1998).

Although sample 10tav04 is interpreted as of enriched terrigenous origin, it may have been reshaped by another component. Turner et al. (1996) found the Ba/Th ratio is indicative of fluids derived by dehydration of subducted oceanic crust. Sample 10tav04 has substantially elevated Ba/Th ratio (825), which, together with its radiogenic $^{87}Sr/^{86}Sr$ values (up to 0.7070), suggests the addition of a Sr-rich fluid (Fig. 11), which has later modified its trace element budget. Its extreme Ba/Th ratio also identifies sample 10tav04 as the only one that has undergone strong fluid metasomatism. Although the Ba/Th ratio of sample 10tav05 is not particularly high (29), its higher carbonate content along with comparable radiogenic $^{87}Sr/^{86}Sr$ to sample 10tav04 suggest it might have also undergone fluid metasomatism, and that its protolith might have been more carbonate-rich, possibly as carbonates atop subducted oceanic crust or decapitated seamounts.

Therefore, the protoliths of the MORB-like group are uniform, whereas the protoliths of the enriched blueschists are evidently affected by a terrigenous component to a differing extent (Figs. 8, 9, and 10) and may have undergone strong Sr-rich fluid metasomatism (sample 10tav04). The protoliths of the enriched group are also oceanic basaltic rocks, but as their geochemical signature is characterized by the presence of a continent-derived terrigenous sedimentary component, they were possibly volcanoclastics.

Fractional crystallization and crustal contamination. The primary tholeiitic magmas of the blueschist protoliths may have experienced considerable fractional crystallization or crustal contamination as indicated by their low Mg-numbers and variable contents of Ni, Cr, and V. REE ratios that are relatively insensitive to fractional crystallization can help to constrain the melting conditions and the source of the magmas (Thirlwall et al. 1994; Miller et al. 1999; Zhu et al. 2015). In Figure 12, all the

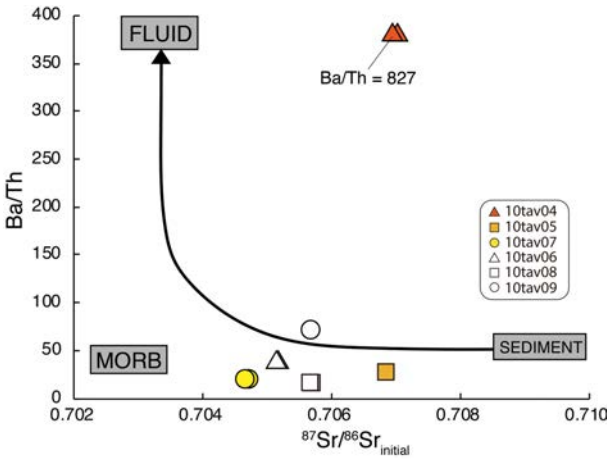

FIGURE 11. $^{87}Sr/^{86}Sr_{initial}$ vs. Ba/Th diagram showing three-component mixing (MORB, sediment, and fluid derived by dehydration of the subducted oceanic crust) to explain the geochemistry of blueschist samples from the Tavşanlı zone (after Turner et al. 1996). Note that sample 10tav04 exhibits distinctly higher Ba/Th ratio (827) than the rest of the samples, suggesting an addition of Sr-rich slab-derived fluid in the source. (Color online.)

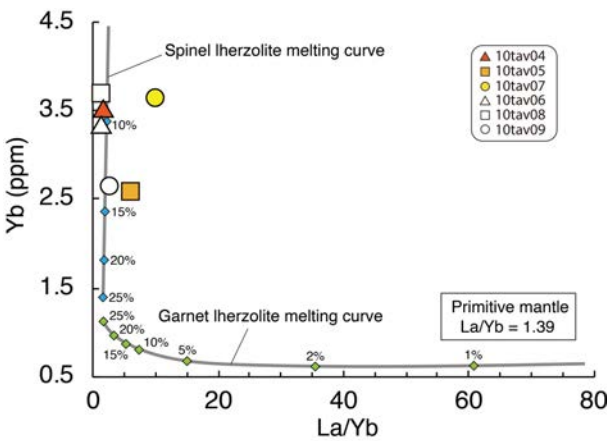

FIGURE 12. La/Yb vs. Yb (ppm) discrimination diagram of blueschist samples from the Tavşanlı zone (partial melting curves calculated from batch melting; adapted from Miller et al. 1999 and Zhu et al. 2015). La and Yb contents of Primitive mantle from Sun and McDonough (1989). All six blueschist samples plot along or parallel to the trajectory for non-modal fractional melts of a spinel peridotitic source, suggesting that the parental magmas of blueschist samples were produced from the differing degrees of partial melting of spinel-facies peridotites. (Color online.)

blueschists plot along or parallel to the trajectory for non-modal fractional melts of a spinel peridotite source rather than that of garnet peridotite (Fig. 12), suggesting that the primary magmas of blueschist samples were produced by differing degrees of partial melting of spinel-facies peridotites, especially the MORB-like group (Miller et al. 1999; Zhu et al. 2015). As summarized by Hofmann et al. (1986), Nb/U and Ce/Pb ratios fall consistently in the ranges 47 ± 10 and 25 ± 5 in mantle-derived oceanic basalts and deviations may indicate crustal contamination or assimilation. Our samples yield variably low Nb/U (8.7–55) and Ce/Pb (1.1–29) values, implying possible minor crustal contamination except for sample 10tav07, which gives Nb/U of 21 and Ce/Pb of 29. Sample 10tav09 exhibits the lowest Nb/U (8.7) and Ce/Pb (1.1) values, indicating the strongest crustal influence. This is more clearly seen in Supplemental[1] Fig. S6 as both high Ba/Rb and low Nb/La are reliable trace element indices of crustal contamination (e.g., Kieffer et al. 2004).

Whole-rock trace element budget for blueschist

To better understand how trace elements are distributed among the mineral inventory of blueschist, we calculated the trace element budgets using average trace element compositions, the modal abundances of the minerals, and the corresponding whole-rock compositions. The modal abundances for minerals were first obtained by point counting in thin sections, then cross checked by least-squares mass balance (Table 1). The calculated elemental distributions are illustrated in Figure 13. It is quite difficult to accurately determine the budgets of all the trace elements (such as Zr and Hf) in blueschists because of their fine grain size, complex mineralogy, and the important yet rare occurrence of accessory minerals (e.g., Spandler et al. 2003). We attribute the imprecise elemental budgets particularly to the lack of data for minor phases rich in key trace elements, such as zircon, phengite, and hematite, but also possibly due to zoning and contamination giving rise to heterogeneous trace element compositions. Nonetheless, the budgets for most elements in the major blueschist phases are well constrained, especially for samples 10tav04 and 07 because of their simpler mineralogy.

Zr and Hf are predominantly accommodated in zircon (e.g., Rubatto 2002; Belousova et al. 2002), which is believed to account for the poor Zr and Hf matches in several samples (Fig. 13). Lawsonite hosts ~50% of REE, nearly all Sr and ~40% of Th in sample 10tav07, with hematite and Mn-garnet being the significant carriers of LREE and HREE, respectively (Fig. 13). In a similar budget estimation for mafic lawsonite blueschist, Spandler et al. (2003) also found lawsonite to be the main host for ~90% of Sr, ~30% of LREE and substantial proportions of Th. Generally, titanite accommodates the majority of Nb, Ta, and Ti, whereas phengite governs the LILE, and sodic amphibole controls Li and Mn, which is in good agreement with previous studies (Fig. 13; Spandler et al. 2003; Martin et al. 2014). Th, U, Sr, and REE are controlled jointly by lawsonite, titanite, apatite, and hematite.

Using the available mineral data, we can reconstruct and compensate the element budgets for the less well-constrained samples. For some phases we only managed to obtain trace element results for one sample (e.g., hematite in 10tav07 and aragonite in 10tav05). In 10tav05, LILE are very poorly constrained because of the lack of phengite data, and in 10tav06, 08, and 09, hematite should account for the discrepancies in Th, U, and LREE. Minor and accessory phases such as apatite, titanite, hematite, and zircon are significant in controlling trace element distributions and can thus affect the trace element behavior dramatically.

Significance of lawsonite geochemistry

Lawsonite is recognized as one of the most significant hydrous minerals in mafic rocks for transporting water and key trace elements (e.g., Sr, Th, U, and REE) to great depths during subduction (Baur 1978; Schmidt 1995; Tribuzio et al. 1996; Spandler et al.

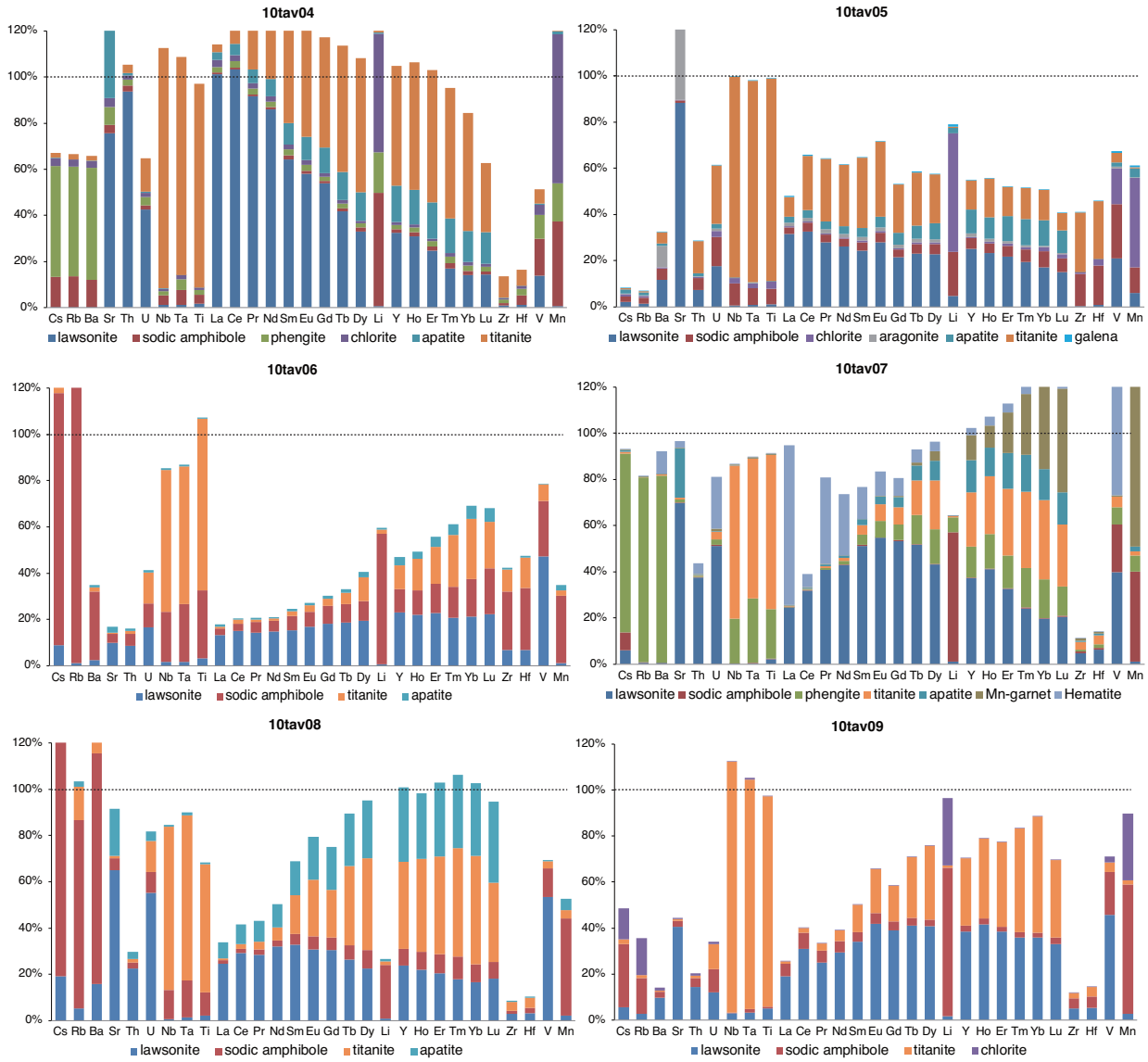

FIGURE 13. Trace element budget for the Tavşanlı zone blueschist samples. See text for details. (Color online.)

2003; Tsujimori et al. 2006; Usui et al. 2007; Martin et al. 2014; Vitale Brovarone et al. 2014). Our results agree well with previous findings and indicate that lawsonite in blueschists of different origins exhibits strong variations in trace element behavior (e.g., Martin et al. 2014).

Generally, lawsonite in the enriched terrigenous blueschists shows higher LREE and Sr than MORB-like blueschists (Figs. 14a and 14b). Allanite usually accounts for La, Ce, Pr, and Nd in blueschists (Hermann 2002; Gieré and Sorensen 2004), but is absent from the blueschists in this study. LREE contents in our lawsonites are thus not compromised by allanite and yield enriched compositions, especially in enriched blueschist samples (10tav04, 05, and 07), where Th and U are strikingly enriched as well (Fig. 5). Pb and Sr are commonly hosted by high-pressure phases such as apatite and aragonite, which should host high Pb/Ce and Sr contents instead of lawsonite (Spandler et al. 2003; Martin et al. 2014). However, lawsonite in 10tav05 exhibits higher Pb/Ce ratio and Sr content than apatite, probably due to the rock's higher degree of alteration and large abundance of aragonite (Figs. 14a and 14b). The negative correlation between Pb/Ce ratio and Ce content in all samples except 10tav05 (Fig. 14a) indicates that lawsonite fails to fractionate Pb from Ce regardless of its origin.

A more distinctive feature is illustrated in Figure 14c: lawsonites in blueschists of continent-derived terrigenous origin exhibit much higher La concentrations and La/Dy ratios than those in MORB-like blueschists. La/Dy ratio correlates positively with La content in all lawsonites, suggesting that lawsonite not only hosts a substantial amount of LREE, but is capable of fractionating LREE (La) from MREE (Dy). Martin et al. (2014) found that lawsonites in metasomatic rocks have elevated La/Dy, La, and Ce contents along with lower Pb/Ce, which is also seen in our sample 10tav04 that is believed to have undergone fluid metasomatism. As for

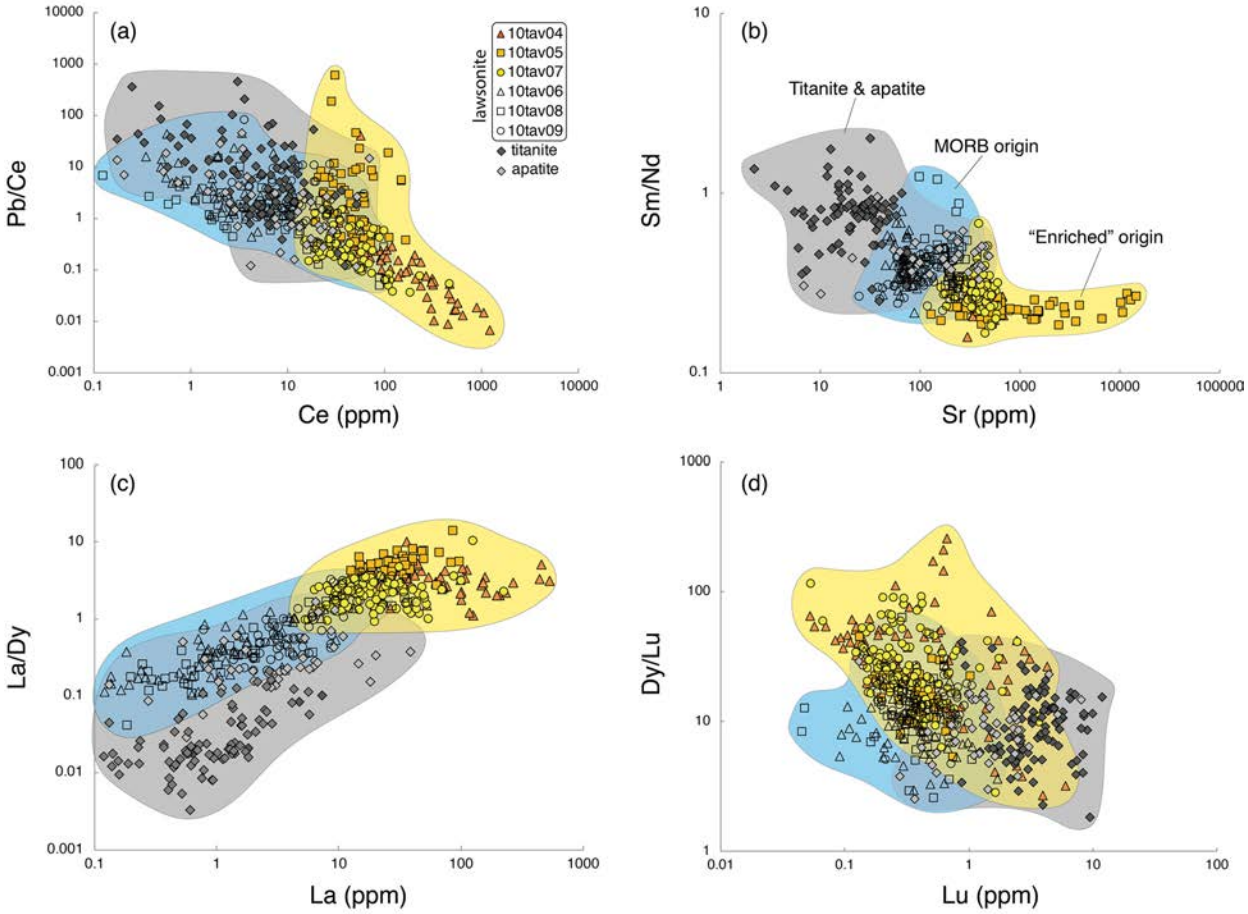

FIGURE 14. (**a**) Pb/Ce vs. Ce (ppm); (**b**) Sm/Nd vs. Sr (ppm); (**c**) La/Dy vs. La (ppm), and (**d**) Dy/Lu vs. Lu (ppm) diagrams for Tavşanlı zone lawsonites. For comparison, titanite (filled diamonds) and apatite (empty diamonds) in blueschist samples from this study are also shown. (Color online.)

HREE, lawsonites in enriched samples yield much higher Dy/Lu ratios than those of MORB origin, which results in a negative REE slope (Fig. 6), whereas titanite and apatite have more enriched Lu concentrations and lower Dy/Lu.

Despite the common major element characteristics of the lawsonites, they show extremely heterogeneous trace element concentrations (Fig. 14). Martin et al. (2014) attributed this to the flexible crystal structure capable of incorporating variable sizes of trace elements. Our study demonstrates that lawsonite is prone to chemical variations that reflect its protolith. Different protoliths give rise to chemically variable lawsonite despite similar parageneses. Trace elements in lawsonites in MORB-like blueschists differ considerably from those with enriched origin, with the latter being more enriched in Sr, Th, U, and LREE, and showing more pronounced LREE/HREE fractionation, indicating the significance of continent-derived terrigenous sediments in shaping the trace element distribution in lawsonite blueschists.

Potential constraints on the origin and geochemistry of potassium-rich magmatism

Key geochemical signature of Mediterranean potassium-rich magmas. Along with the high K_2O content, strongly enriched incompatible elements, elevated $^{87}Sr/^{86}Sr$, $^{207}Pb/^{204}Pb$, $^{187}Os/^{188}Os$, and low $^{143}Nd/^{144}Nd$ and $^{176}Hf/^{177}Hf$ ratios, the extremely high Th/La ratio has recently been recognized to uniquely fingerprint magmas of the Alpine-Himalayan Orogenic Belt (AHOB; Tommasini et al. 2011; Prelević et al. 2013; Wang et al. 2017). For most mantle-derived magmas, Th/La ratios are no larger than 0.5 (Fig. 15), because it is difficult to fractionate Th from La by either dehydration or melting processes that carry slab material to the arc source (Plank 2005). Tommasini et al. (2011) proposed that the strikingly high Th/La signature of Tethyan Realm lamproites could be explained by lawsonite and zoisite/epidote veins and segregations in chaotic mélange domains accreted to the Eurasian plate during collisional events. This argument is echoed by Prelević et al. (2013), who reported the same extreme Th/La ratios in the Mediterranean and Tibetan post-collisional (but not lamproitic) mafic lavas, and they also attributed it to the possible presence of a blueschist facies end-member including lawsonite and zoisite veins.

Unraveling the high Th/La enigma. We here demonstrate that lawsonites with differing origins in the Tavşanlı zone blueschists have distinct Th/La fractionation characteristics (Fig. 15): lawsonites with enriched continent-derived terrigenous origin show similar Th/La vs. Sm/La to AHOB lavas, whereas those

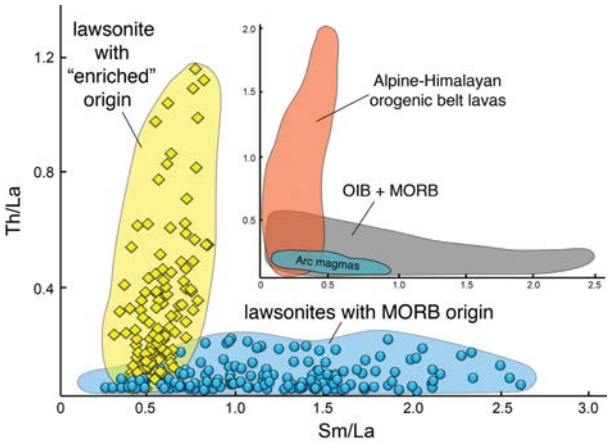

FIGURE 15. Th/La vs. Sm/La comparison of lawsonite in blueschist sample 10tav07 (enriched terrigenous origin) and in the blueschists of MORB origin with Alpine-Himalayan Orogenic Belt lavas (Wang et al. 2017), OIB (GEOROC database, http://georoc.mpch-mainz.gwdg.de/georoc), MORB (GEOROC database, http://georoc.mpch-mainz.gwdg.de/georoc), and arc magmas related to slab-derived mantle metasomatism (data from Tommasini et al. 2011 and references therein). Note the distinction between "enriched" and MORB-like lawsonites is as striking as that between AHOB and other lavas. (Color online.)

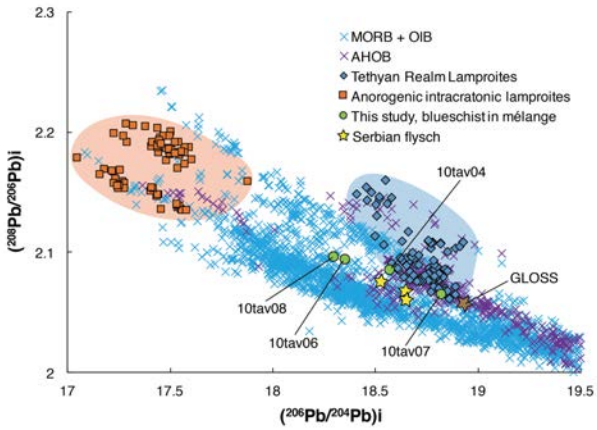

FIGURE 16. ($^{208}Pb/^{206}Pb$)i vs. ($^{206}Pb/^{204}Pb$)i variation of lawsonite blueschists in the Tavşanlı zone melange, AHOB lavas, Tethyan Realm lamproites, and anorogenic intracratonic lamproites along with MORBs and OIBs, adapted from Tommasini et al. (2011). Also shown are GLOSS and Serbian flysch. MORB and OIB data from Stracke et al. (2003) and GEOROC database, data for Tethyan Realm lamproites and anorogenic intracratonic lamproites from Tommasini et al. (2011), AHOB data from GEOROC database, Serbian flysch data from Prelević and Foley (2007), and GLOSS data from Plank and Langmuir (1998). (Color online.)

with MORB-like origin are similar to OIB, MORB, and arc magmas. In other words, not all lawsonite blueschists can account for the unique Th/La ratios observed in AHOB magmas, but only those with terrigenous input. Melting of mélange that contains lawsonite blueschist with enriched terrigenous origin is thus the most appealing explanation of the trace element characteristics of the Mediterranean and AHOB potassium-rich magmatism in a realistic geodynamic setting.

Pb isotope geochemistry supports an important role of lawsonite blueschist in the elevated Th/La ratios. Th/La ratios of both the blueschist whole-rocks and lawsonites yield strongly heterogeneous values where the most elevated Th/La ratios correspond to the continent-derived terrigenous geochemical component (Fig. 16). The most radiogenic $^{206}Pb/^{204}Pb$, $^{207}Pb/^{204}Pb$, and $^{208}Pb/^{204}Pb$ occur in the enriched blueschists (Fig. 9), with 10tav07 showing similar isotopic compositions to GLOSS (Fig. 16). The Pb isotope compositions of Tethyan lamproites and AHOB lavas plot above the mantle array (MORBs and OIBs in Fig. 16), indicating an end-member with considerable time-integrated enrichment of thorogenic Pb isotopes, and their decoupling from uranogenic isotopes (Tommasini et al. 2011). This end-member also has high Th/La. The most enriched blueschist sample (10tav07) does not plot close to this hypothetical end-member, and the less enriched blueschist samples plot toward the mantle array and MORB compositions along a hyperbolic mixing line (Fig. 16), but it should be stressed that we only have the age of metamorphism to constrain the initial Pb isotope compositions of the blueschists (the protolith of the blueschist must be older than its metamorphic age of ~80 Ma). So hypothetically, if the blueschist protoliths, especially those with the enriched crust-like origin, have a much older formation age (Tommasini et al. 2011), they could account for the Pb isotope evolution of Tethyan lamproites and AHOB lavas. These enriched blueschists have similar Pb isotopic affinities to GLOSS, whose present-day Pb isotopic compositions can be used to successfully explain the Pb isotope evolution of Tethyan lamproites (Fig. 9 in Tommasini et al. 2011). Thus, only the blueschists with enriched origin from the melange have the potential to provide the geochemical ingredient responsible for the continental crust-like composition and elevated Th/La ratios in the AHOB lavas.

Melting of a newly formed lithosphere. The Alpine-Himalayan orogenic belt resulted from a long-lasting convergence between Eurasia and Gondwana, beginning in the Permian. This convergence involved accretion of thin continental slivers that mostly originated by rifting from northern Gondwanaland, and numerous oceanic island arcs, which eventually formed an orogenic system consisting of multiple belts. The net effect of this accretion was a complex interfingering of geologically and geochemically contrasting compositions, resulting in a very heterogeneous lithospheric mantle under the Mediterranean region. Generally, the mantle might be heavily metasomatized by melts derived from subducted continent-derived terrigenous sediments (e.g., Prelević et al. 2013), and melting of this metasomatized source accounts for the widespread orogenic fingerprint identified in potassium-rich post-collisional magmas (e.g., Prelević et al. 2008, 2013; Lustrino et al. 2011).

At least some part of this mantle is newly formed during accretion of microplates or other small continental blocks, composed of a mixture of strongly depleted forearc peridotites, oceanic crust, and oceanic and continental sediments (Prelević et al. 2008; Gonzalez et al. 2015; Wang et al. 2017). However, the significance of new lithosphere of this type, in which blueschist mélange and other blocks are all imbricated together, is often underestimated or overlooked when investigating the origin of potassium-rich orogenic magmatism.

Here, we tentatively propose that the unique high Th/La

signature seen in AHOB potassium-rich magmas could be derived from lawsonite blueschist with continent-derived terrigenous origin. This Th/La signature could be imparted to the lavas by melting of newly formed lithosphere that contains mélanges including blueschists imbricated together with other types of rocks at shallow levels (<80 km). Unlike Andean-style subduction where a succession of additional reactions would modify and dilute the Th/La signature, shallow tectonic imbrication preserves many of the geochemical characteristics and stores them in the new lithosphere. However, the high Th/La signature is not conveyed by a single-stage process from lawsonite blueschist to ensuing magmas as proposed previously (Wang et al. 2017) but probably results from a series of metamorphic and magmatic processes that steadily increase the Th/La ratio.

Mediterranean potassium-rich magmatism may be triggered by two major factors, namely the roll-back of the underthrust lithospheric slab that causes post-collisional extension, collapse of the orogenic belts, and large-scale elevation of several orogenic massifs, combined with the initiation and progression of a slab tear (e.g., Prelević et al. 2015 and references therein). Before the continental lithosphere blocks collided, intra-oceanic subduction induced by the closure of small ocean basins gave rise to many geological events in the Mediterranean region during the Mesozoic. This closure of small ocean basins may result in obduction of ophiolites onto a passive margin or accretionary uplift and collision of continental blocks, resulting in the thickened continental crust. Melange that includes blueschists on the interface between the subducting oceanic slab and the overlying mantle are likely to imbricate with oceanic crust chunks at ~60–80 km (e.g., Fig. 8 in Gonzalez et al. 2015; Fig. 11 in Wang et al. 2017). Heat from the convecting mantle after slab break-off or lithospheric delamination and slab roll-back would preferentially melt previously enriched domains (mélanges) stored at shallow depths within the lithospheric mantle. The preferential melting of fertile, enriched components results in the generation of potassium-rich mafic magmas with diagnostic geochemical characteristics.

Implications

This study provides a new, comprehensive geochemical data set of whole-rock major and trace element compositions and the first radiogenic isotopic measurements on eastern Mediterranean lawsonite blueschists. This allows us to recognize two groups of blueschist with differing protoliths of MORB-like and continent-derived terrigenous origin. As the most important hydrous mineral in hosting Th, U, Sr, and LREE in blueschist, lawsonite has great potential to explain the enigmatic geochemistry of Mediterranean potassium-rich magmatism because it is the only mineral that can carry the unusually high Th/La signature, which is unique to Alpine-Himalayan orogenic belt (AHOB) potassium-rich magmas (Fig. 15). However, only those lawsonite blueschists with continental input can explain this Th/La feature.

Given the significance of lawsonite blueschist in transporting such a unique signature, mélange should be considered when discussing the geodynamics of magma origin, as this is an environment where subducted sediments, oceanic crust, blueschist, and mantle peridotite are tectonically imbricated together.

Trace element data of lawsonite blueschist in the AHOB is scarce, hindering acceptance of the hypothesis that blueschist-bearing mélange is important. However, the extremely high Th/La feature has not been observed in any minerals other than lawsonite, and all accessory minerals can be discounted. Lawsonite has also been reported to carry a high Th/La signature (up to 4.88) from nearby Sivrihisar in Turkey and Alpine Corsica in France (Vitale Brovarone et al. 2014; Martin et al. 2014). It is thus reasonable to link lawsonite blueschist to the genesis of AHOB potassium-rich magmatism and to consider the melting of newly formed lithosphere that contains blueschist-bearing mélanges in other areas.

Funding

This work was supported by the Strategic Priority Research Program (B) of Chinese Academy of Sciences (Grant No. XDB18000000), National Natural Science Foundation of China (Grant No. 41773055) and the ARC Centre of Excellence for Core to Crust Fluid Systems/GEMOC. This is contribution 1305 from the ARC Centre of Excellence for Core to Crust Fluid Systems (http://www.ccfs.mq.edu.au) and 1296 in the GEMOC Key Centre (http://www.gemoc.mq.edu.au). The Macquarie University HDR Fund supported experimental and analytical work. Fieldwork in Turkey was funded by the Deutsche Forschungsgemeinschaft.

Acknowledgments

We are very grateful to Steve Galer, Heinz Feldmann, Reimund Jotter, and Peter Wieland for their help with isotope measurements. Regina Mertz, Will Powell, David Adams, and Norman Pearson are thanked for their instruction during laser and microprobe analyses. Simone Tommasini and Alexis Plunder gave insightful comments on an early version of this manuscript. We appreciate Estibalitz Ukar and an anonymous reviewer for their constructive reviews and the editorial support of Gregory Dumond.

References cited

Agard, P., Yamato, P., Jolivet, L., and Burov, E. (2009) Exhumation of oceanic blueschists and eclogites in subduction zones: timing and mechanisms. Earth-Science Reviews, 92(1-2), 53–79.

Altunkaynak, Ş., and Genç, Ş.C. (2008) Petrogenesis and time-progressive evolution of the Cenozoic continental volcanism in the Biga Peninsula, NW Anatolia (Turkey). Lithos, 102(1-2), 316–340.

Baur, W.H. (1978) Crystal structure refinement of lawsonite. American Mineralogist, 63, 311–315.

Becker, H., Jochum, K.P., and Carlson, R.W. (2000) Trace element fractionation during dehydration of eclogites from high-pressure terranes and the implications for element fluxes in subduction zones. Chemical Geology, 163(1), 65–99.

Beinlich, A., Klemd, R., John, T., and Gao, J. (2010) Trace-element mobilization during Ca-metasomatism along a major fluid conduit: Eclogitization of blueschist as a consequence of fluid–rock interaction. Geochimica et Cosmochimica Acta, 74(6), 1892–1922.

Belousova, E., Griffin, W.L., O'Reilly, S.Y., and Fisher, N.L. (2002) Igneous zircon: trace element composition as an indicator of source rock type. Contributions to Mineralogy and Petrology, 143(5), 602–622.

Bernard-Griffiths, J., Carpenter, M.S.N., Peucat, J.J., and Jahn, B.M. (1986) Geochemical and isotopic characteristics of blueschist facies rocks from the Île de Groix, Armorican Massif (northwest France). Lithos, 19(3), 235–253.

Bulle, F., Bröcker, M., Gärtner, C., and Keasling, A. (2010) Geochemistry and geochronology of HP mélanges from Tinos and Andros, cycladic blueschist belt, Greece. Lithos, 117(1-4), 61–81.

Çelik, Ö.F., Chiaradia, M., Marzoli, A., Özkan, M., Billor, Z., and Topuz, G. (2016) Jurassic metabasic rocks in the Kızılırmak accretionary complex (Kargı region, Central Pontides, Northern Turkey). Tectonophysics, 672, 34–49.

Çetinkaplan, M., Candan, O., Oberhänsli, R., and Bousquet, R. (2008) Pressure-temperature evolution of lawsonite eclogite in Sivrihisar; Tavşanlı Zone-Turkey. Lithos, 104(1-4), 12–32.

Cloos, M., and Shreve, R.L. (1988) Subduction-channel model of prism accretion, melange formation, sediment subduction, and subduction erosion at convergent plate margins: 1. Background and description. Pure and Applied Geophysics, 128(3-4), 455–500.

Collins, A.S., and Robertson, A.H.F. (1997) Lycian melange, southwestern Turkey: an emplaced Late Cretaceous accretionary complex. Geology, 25(3), 255–258.

Conticelli, S. (1998) The effect of crustal contamination on ultrapotassic magmas with lamproitic affinity: mineralogical, geochemical and isotope data from the Torre Alfina lavas and xenoliths, Central Italy. Chemical Geology, 149(1), 51–81.

Conticelli, S., D'Antonio, M., Pinarelli, L., and Civetta, L. (2002) Source con-

tamination and mantle heterogeneity in the genesis of Italian potassic and ultrapotassic volcanic rocks: Sr–Nd–Pb isotope data from Roman Province and Southern Tuscany. Mineralogy and Petrology, 74(2-4), 189–222.

Davis, P.B., and Whitney, D.L. (2006) Petrogenesis of lawsonite and epidote eclogite and blueschist, Sivrihisar Massif, Turkey. Journal of Metamorphic Geology, 24(9), 823–849.

Dubacq, B., and Plunder, A. (2018) Controls on trace element distribution in oxides and silicates. Journal of Petrology, 59(2), 233–256.

Ernst, W.G. (1988) Tectonic history of subduction zones inferred from retrograde blueschist *P-T* paths. Geology, 16, 1081–1084.

Fornash, K.F., Cosca, M.A., and Whitney, D.L. (2016) Tracking the timing of subduction and exhumation using $^{40}Ar/^{39}Ar$ phengite ages in blueschist- and eclogite-facies rocks (Sivrihisar, Turkey). Contributions to Mineralogy and Petrology, 171(7), 67.

Fotoohi Rad, G.R., Droop, G.T.R., Amini, S., and Moazzen, M. (2005) Eclogites and blueschists of the Sistan Suture Zone, eastern Iran: A comparison of P-T histories from a subduction mélange. Lithos, 84(1-2), 1–24.

Fryer, P., Wheat, C.G., and Mottl, M.J. (1999) Mariana blueschist mud volcanism: Implications for conditions within the subduction zone. Geology, 27(2), 103–106.

Galer, S.J.G. (1999) Optimal double and triple spiking for high precision lead isotopic measurement. Chemical Geology, 157(3), 255–274.

Ge, M.-h., Zhang, J.-j., Liu, K., Ling, Y.-y., Wang, M., and Wang, J.-m. (2016) Geochemistry and geochronology of the blueschist in the Heilongjiang Complex and its implications in the late Paleozoic tectonics of eastern NE China. Lithos, 261, 232–249.

Gieré, R., and Sorensen, S.S. (2004) Allanite and other REE-rich epidote-group minerals. Reviews in Mineralogy and Geochemistry, 56, 431–493.

Goffe, B., Michard, A., Kienast, J.R., and Le Mer, O. (1988) A case of obduction-related high-pressure, low-temperature metamorphism in upper crustal nappes, Arabian continental margin, Oman: *P-T* paths and kinematic interpretation. Tectonophysics, 151, 363–386.

Göncüoglu, M.C., Yalınız, M.K., and Tekin, U.K. (2006) Geochemistry, tectono-Magmatic discrimination and radiolarian ages of basic extrusives within the Izmir-Ankara Suture Belt (NW Turkey): Time constraints for the Neotethyan evolution. Ofioliti, 31(1), 25–38.

Göncüoglu, M.C., Sayit, K., and Tekin, U.K. (2010) Oceanization of the northern Neotethys: Geochemical evidence from ophiolitic melange basalts within the İzmir–Ankara suture belt, NW Turkey. Lithos, 116(1), 175–187.

Gonzalez, C.M., Gorczyk, W., and Gerya, T.V. (2015) Decarbonation of subducting slabs: Insight from petrological–thermomechanical modeling. Gondwana Research, 36, 314–332.

Guo, Z. et al. (2014) The role of subduction channel mélanges and convergent subduction systems in the petrogenesis of post-collisional K-rich mafic magmatism in NW Tibet. Lithos, 198-199, 184–201.

Haggerty, S.E., Fung, A.T., and Burt, D.M. (1994) Apatite, phosphorus and titanium in eclogitic garnet from the upper mantle. Geophysical Research Letters, 21(16), 1699–1702.

Harris, R.A., Sawyer, R.K., and Audley-Charles, M.G. (1998) Collisional melange development: Geologic associations of active melange-forming processes with exhumed melange facies in the western Banda orogen, Indonesia. Tectonics, 17(3), 458–479.

Hart, S.R. (1984) A large-scale isotope anomaly in the Southern Hemisphere mantle. Nature, 309(5971), 753.

Hauri, E.H., Wagner, T.P., and Grove, T.L. (1994) Experimental and natural partitioning of Th, U, Pb and other trace elements between garnet, clinopyroxene and basaltic melts. Chemical Geology, 117(1-4), 149–166.

Hermann, J. (2002) Allanite: thorium and light rare earth element carrier in subducted crust. Chemical Geology, 192(3-4), 289–306.

Hofmann, A.W., Jochum, K.P., Seufert, M., and White, W.M. (1986) Nb and Pb in oceanic basalts: new constraints on mantle evolution. Earth and Planetary Science Letters, 79(1), 33–45.

Honegger, K., Le Fort, P., Mascle, G., and Zimmermann, J.L. (1989) The blueschists along the Indus Suture Zone in Ladakh, NW Himalaya. Journal of Metamorphic Geology, 7(1), 57–72.

Jochum, K.P. et al. (2011) Determination of reference values for NIST SRM 610-617 glasses following ISO guidelines. Geostandards and Geoanalytical Research, 35(4), 397–429.

Karson, J.A. (2002) Geologic structure of the uppermost oceanic crust created at fast-to intermediate-rate spreading centers. Annual Review of Earth and Planetary Sciences, 30(1), 347–384.

Kieffer, B., Arndt, N. Lapierre, H., Bastien, F., Bosch, D., Pecher, A., Yirgu, G., Ayalew, D., Weis, D., and Jerram, D.A (2004), Flood and Shield Basalts from Ethiopia: Magmas from the African Superswell. Journal of Petrology, 45(4), 793–834(742).

King, R.L., Bebout, G.E., Moriguti, T., and Nakamura, E. (2006) Elemental mixing systematics and Sr–Nd isotope geochemistry of mélnge formation: Obstacles to identification of fluid sources to arc volcanics. Earth and Planetary Science Letters, 246(3), 288–304.

Kim, D., Katayama, I., Wallis, S., Michibayashi, K., Miyake, A., Seto, Y., and Azuma, S. (2015) Deformation microstructures of glaucophane and lawsonite in experimentally deformed blueschists: Implications for intermediate-depth intraplate earthquakes. Journal of Geophysical Research: Solid Earth, 120(2), 1229–1242.

Kleine, B.I., Skelton, A.D.L., Huet, B., and Pitcairn, I.K. (2014) Preservation of blueschist-facies minerals along a shear zone b coupled metasomatism and fast-flowing CO_2-bearing fluids. Journal of Petrology, 55(10), 1905–1939.

Klemd, R. (2013) Metasomatism during high-pressure metamorphism: eclogites and blueschist-facies rocks, metasomatism and the chemical transformation of rock. Lecture Notes in Earth System Sciences, pp. 351–413. Springer.

Klemme, S., Blundy, J.D., and Wood, B.J. (2002) Experimental constraints on major and trace element partitioning during partial melting of eclogite. Geochimica et Cosmochimica Acta, 66(17), 3109–3123.

Leake, B.E., Woolley, A.R., Arps, C.E.S., Birch, W.D., Gilbert, M.C., Grice, J.D., Hawthorne, F.C., Kato, A., Kisch, H.J., and Krivovichev, V.G. (1997) Report. Nomenclature of amphiboles: report of the subcommittee on amphiboles of the international mineralogical association commission on new minerals and mineral names. Mineralogical Magazine, 61(2), 295–321.

Lugmair, G.W., and Galer, S.J.G. (1992) Age and isotopic relationships among the angrites Lewis Cliff 86010 and Angra dos Reis. Geochimica et Cosmochimica Acta, 56(4), 1673–1694.

Lugmair, G.W., and Marti, K. (1978) Lunar initial $^{143}Nd/^{144}Nd$: Differential evolution of the lunar crust and mantle. Earth and Planetary Science Letters, 39(3), 349–357.

Lustrino, M., Duggen, S., and Rosenberg, C.L. (2011) The Central-Western Mediterranean: anomalous igneous activity in an anomalous collisional tectonic setting. Earth-Science Reviews, 104(1), 1–40.

Maekawa, H., Shozul, M., Ishii, T., Fryer, P., and Pearce, J.A. (1993) Blueschist Metamorphism in an Active Subduction Zone. Nature, 364, 520–523.

Martin, L.A.J., Hermann, J., Gauthiez-Putallaz, L., Whitney, D.L., Vitale Brovarone, A., Fornash, K.F., and Evans, N.J. (2014) Lawsonite geochemistry and stability implication for trace element and water cycles in subduction zones. Journal of Metamorphic Geology, 32(5), 455–478.

Martin, L.A.J., Wood, B.J., Turner, S., and Rushmer, T. (2011) Experimental Measurements of Trace Element Partitioning Between Lawsonite, Zoisite and Fluid and their Implication for the Composition of Arc Magmas. Journal of Petrology, 52(6), 1049–1075.

Maruyama, S., Liou, J.G., and Terabayashi, M. (1996) Blueschists and eclogites of the world and their exhumation. International Geology Review, 38(6), 485–594.

Maulana, A., Christy, A.G., Ellis, D.J., Imai, A., and Watanabe, K. (2013) Geochemistry of eclogite- and blueschist-facies rocks from the Bantimala Complex, South Sulawesi, Indonesia: Protolith origin and tectonic setting. Island Arc, 22(4), 427–452.

Miller, C., Schuster, R., Klötzli, U., Frank, W., and Purtscheller, F. (1999) Post-collisional potassic and ultrapotassic magmatism in SW Tibet: geochemical and Sr–Nd–Pb–O isotopic constraints for mantle source characteristics and petrogenesis. Journal of Petrology, 40(9), 1399–1424.

Miller, D.P., Marschall, H.R., and Schumacher, J.C. (2009) Metasomatic formation and petrology of blueschist-facies hybrid rocks from Syros (Greece): Implications for reactions at the slab–mantle interface. Lithos, 107(1-2), 53–67.

Mulcahy, S.R., Vervoort, J.D., and Renne, P.R. (2014) Dating subduction zone metamorphism with combined garnet and lawsonite Lu-Hf geochronology. Journal of Metamorphic Geology, 32(5), 515–533.

Okay, A.I. (1978) Sodic pyroxenes from metabasites in the eastern Mediterranean. Contributions to Mineralogy and Petrology, 68(1), 7–11.

——— (1980a) Mineralogy, petrology, and phase relations of glaucophane-lawsonite zone blueschists from the Tavşanli Region, Northwest Turkey. Contributions to Mineralogy and Petrology, 72(3), 243–255.

——— (1980b) Lawsonite zone blueschists and a sodic amphibole producing reaction in the Tavşanli Region, Northwest Turkey. Contributions to Mineralogy and Petrology, 75(3), 179–186.

——— (1982) Incipient blueschist metamorphism and metasomatism in the Tavşanli region, Northwest Turkey. Contributions to Mineralogy and Petrology, 79(4), 361–367.

——— (1986) High-pressure/low-temperature metamorphic rocks of Turkey. Geological Society of America Memoirs, 164, 333–347.

——— (1989) Alpine-Himalayan Blueschists. Annual Review of Earth and Planetary Sciences, 17(1), 55–87.

——— (2002) Jadeite-chloritoid-glaucophane-lawsonite blueschists in north-west Turkey: unusually high P/T ratios in continental crust. Journal of Metamorphic Geology, 20(8), 757–768.

Okay, A.I., and Tüysüz, O. (1999) Tethyan sutures of northern Turkey. Geological Society, London, Special Publications, 156(1), 475–515.

Okay, A.I., and Whitney, D.L. (2010) Blueschists, eclogites, ophiolites and suture zones in northwest Turkey: A review and a field excursion guide. Ofioliti, 35(2), 131–171.

Okay, A.I., Harris, N.B.W., and Kelley, S.P. (1998) Exhumation of blueschists along a Tethyan suture in northwest Turkey. Tectonophysics, 285(3-4), 275–299.

Okazaki, K., and Hirth, G. (2016) Dehydration of lawsonite could directly trigger earthquakes in subducting oceanic crust. Nature, 530, 81–84.

Özbey, Z., Ustaömer, T., and Robertson, A.H.F. (2013) Mesozoic magmatic and sedimentary development of the Tavşanlı Zone (NW Turkey): implications for rifting, passive margin development and ocean crust emplacement. Geological Society, London, Special Publications, 372.

Pagé, L., Hattori, K., de Hoog, J.C.M., and Okay, A.I. (2016) Halogen (F, Cl, Br, I) behaviour in subducting slabs: A study of lawsonite blueschists in western Turkey. Earth and Planetary Science Letters, 442, 133–142.

Palin, R.M., and White, R.W. (2015) Emergence of blueschists on Earth linked to secular changes in oceanic crust composition. Nature Geoscience, 9, 60–64.

Parkinson, C.D. (1996) The origin and significance of metamorphosed tectonic blocks in mélanges: evidence from Sulawesi, Indonesia. Terra Nova, 8(4), 312–323.

Patočka, F., and Pin, C. (2005) Sm-Nd isotope and trace element evidence for heterogeneous igneous protoliths of Variscan mafic blueschists in the East Krkonoše Complex (West Sudetes, NE Bohemian Massif, Czech Republic). Geodinamica Acta, 18(5), 363–374.

Pearce, J.A. (1975) Basalt geochemistry used to investigate past tectonic environments on Cyprus. Tectonophysics, 25(1), 41–67.

——— (1983) The role of sub-continental lithosphere in magma genesis at destructive plate margins. Continental Basalts & Mantle Xenoliths, 147(6), 2162–2173.

Pearce, J.A., and Cann, J.R. (1973) Tectonic Setting of Basic Volcanic Rocks determined using Trace Element Analyses. Earth & Planetary Science Letters, 19(2), 290–300.

Peccerillo, A., and Martinotti, G. (2006) The Western Mediterranean lamproitic magmatism: origin and geodynamic significance. Terra Nova, 18(2), 109–117.

Plank, T. (2005) Constraints from thorium/lanthanum on sediment recycling at subduction zones and the evolution of the continents. Journal of Petrology, 46(5), 921–944.

Plank, T., and Langmuir, C.H. (1998) The chemical composition of subducting sediment and its consequences for the crust and mantle. Chemical Geology, 145(3-4), 325–394.

Plunder, A., Agard, P., Chopin, C., and Okay, A.I. (2013) Geodynamics of the Tavşanlı zone, western Turkey: Insights into subduction/obduction processes. Tectonophysics, 608(0), 884–903.

Plunder, A., Agard, P., Chopin, C., Pourteau, A., and Okay, A.I. (2015) Accretion, underplating and exhumation along a subduction interface: From subduction initiation to continental subduction (Tavşanlı zone, W. Turkey). Lithos, 226(0), 233–254.

Plunder, A., Agard, P., Chopin, C., Soret, M., Okay, A.I., and Whitechurch, H. (2016) Metamorphic sole formation, emplacement and blueschist facies overprint: early subduction dynamics witnessed by western Turkey ophiolites. Terra Nova, 28(5), 329–339.

Poli, S., and Schmidt, M.W. (1997) The high-pressure stability of hydrous phases in orogenic belts: an experimental approach on eclogite-forming processes. Tectonophysics, 273(1-2), 169–184.

Pourteau, A., Candan, O., and Oberhänsli, R. (2010) High-pressure metasediments in central Turkey: Constraints on the Neotethyan closure history. Tectonics, 29(5), TC5004.

Pourteau, A., Sudo, M., Candan, O., Lanari, P., Vidal, O., and Oberhänsli, R. (2013) Neotethys closure history of Anatolia: insights from ^{40}Ar-^{39}Ar geochronology and *P-T* estimation in high-pressure metasedimentary rocks. Journal of Metamorphic Geology, 31(6), 585–606.

Prelević, D., and Foley, S.F. (2007) Accretion of arc-oceanic lithospheric mantle in the Mediterranean: Evidence from extremely high-Mg olivines and Cr-rich spinel inclusions in lamproites. Earth and Planetary Science Letters, 256(1-2), 120–135.

Prelević, D., Foley, S.F., Romer, R., and Conticelli, S. (2008) Mediterranean Tertiary lamproites derived from multiple source components in postcollisional geodynamics. Geochimica et Cosmochimica Acta, 72(8), 2125–2156.

Prelević, D., Jacob, D.E., and Foley, S.F. (2013) Recycling plus: A new recipe for the formation of Alpine-Himalayan orogenic mantle lithosphere. Earth and Planetary Science Letters, 362, 187–197.

Prelević, D., Akal, C., Romer, R.L., Mertz-Kraus, R., and Helvacı, C. (2015) Magmatic response to slab tearing: Constraints from the Afyon Alkaline Volcanic Complex, Western Turkey. Journal of Petrology, 56(3), 527–562.

Raymond, L.A. (1984) Classification of melanges. Geological Society of America Special Papers, 198, 7–20.

Rollinson, H.R. (2014) Using Geochemical Data: Evaluation, Presentation, Interpretation. Routledge, London.

Rojay, B., Altıner, D., Altıner, S.Ö., Pırıl Önen, A., James, S., and Thirlwall, M.F. (2004) Geodynamic significance of the Cretaceous pillow basalts from North Anatolian Ophiolitic Mélange Belt (Central Anatolia, Turkey): geochemical and paleontological constraints. Geodinamica Acta, 17(5), 349–361.

Rubatto, D. (2002) Zircon trace element geochemistry: partitioning with garnet and the link between U–Pb ages and metamorphism. Chemical Geology, 184(1), 123–138.

Saunders, A.D., Norry, M.J., and Tarney, J. (1988) Origin of MORB and chemically-depleted mantle reservoirs: Trace element constraints. Journal of Petrology, Special Volume, 1, 415–445.

Schmidt, M.W. (1995) Lawsonite: Upper pressure stability and formation of higher density hydrous phases. American Mineralogist, 80(11-12), 1286–1292.

Schmidt, M.W., and Poli, S. (1994) The stability of lawsonite and zoisite at high pressures: Experiments in CASH to 92 kbar and implications for the presence of hydrous phases in subducted lithosphere. Earth and Planetary Science Letters, 124(1-4), 105–118.

Schumacher, J.C. (1997) Appendix 2: the estimation of ferric iron in electron microprobe analysis of amphiboles. Mineralogical Magazine, 61(405), 312–321.

Seaton, N.C.A., Whitney, D.L., Teyssier, C., Toraman, E., and Heizler, M.T. (2009) Recrystallization of high-pressure marble (Sivrihisar, Turkey). Tectonophysics, 479, 241–253.

Searle, M., Waters, D.J., Martin, H.N., and Rex, D.C. (1994) Structure and metamorphism of blueschist-eclogite facies rocks from the northeastern Oman Mountains. Journal of the Geological Society, 151, 555–576.

Şengör, A.M., and Yilmaz, Y. (1981) Tethyan evolution of Turkey: a plate tectonic approach. Tectonophysics, 75(3), 181–241.

Sherlock, S., Kelley, S., Inger, S., Harris, N., and Okay, A. (1999) ^{40}Ar-^{39}Ar and Rb-Sr geochronology of high-pressure metamorphism and exhumation history of the Tavşanlı Zone, NW Turkey. Contributions to Mineralogy and Petrology, 137(1-2), 46–58.

Shervais, J.W. (1982) Ti-V plots and the petrogenesis of modern and ophiolitic lavas. Earth and Planetary Science Letters, 59(1), 101–118.

Song, S., Niu, Y., Zhang, L., Wei, C., Liou, J.G., and Su, L. (2009) Tectonic evolution of early Paleozoic HP metamorphic rocks in the North Qilian Mountains, NW China: New perspectives. Journal of Asian Earth Sciences, 35(3), 334–353.

Sorensen, S.S., Grossman, J.N., and Perfit, M.R. (1997) Phengite-hosted LILE enrichment in eclogite and related rocks: Implications for fluid-mediated mass transfer in subduction zones and arc magma genesis. Journal of Petrology, 38(1), 3–34.

Spandler, C., Hermann, J., Arculus, R., and Mavrogenes, J. (2003) Redistribution of trace elements during prograde metamorphism from lawsonite blueschist to eclogite facies; implications for deep subduction-zone processes. Contributions to Mineralogy and Petrology, 146(2), 205–222.

Steiger, R.H., and Jäger, E. (1977) Subcommission on geochronology: Convention on the use of decay constants in geo- and cosmochronology. Earth and Planetary Science Letters, 36(3), 359–362.

Stern, R.J. (2005) Evidence from ophiolites, blueschists, and ultrahigh-pressure metamorphic terranes that the modern episode of subduction tectonics began in Neoproterozoic time. Geology, 33(7), 557–560.

Stracke, A., Bizimis, M., and Salters, V.J.M. (2003) Recycling oceanic crust: Quantitative constraints. Geochemistry, Geophysics, Geosystems, 4(3), 8003.

Sun, S.S., and McDonough, W.F. (1989) Chemical and isotopic systematics of oceanic basalts: implications for mantle composition and processes. Geological Society, London, Special Publications, 42(1), 313–345.

Tang, X.-C., and Zhang, K.-J. (2013) Lawsonite- and glaucophane-bearing blueschists from NW Qiangtang, northern Tibet, China: mineralogy, geochemistry, geochronology, and tectonic implications. International Geology Review, 56(2), 150–166.

Tankut, A., Dilek, Y., and Önen, P. (1998) Petrology and geochemistry of the Neo-Tethyan volcanism as revealed in the Ankara melange, Turkey. Journal of Volcanology and Geothermal Research, 85(1), 265–284.

Thirlwall, M.F., Upton, B.G.J., and Jenkins, C. (1994), Interaction between continental lithosphere and the Iceland plume—Sr-Nd-Pb isotope geochemistry of Tertiary basalts. NE Greenland, Journal of Petrology, 35(3), 839–879.

Tommasini, S., Avanzinelli, R., and Conticelli, S. (2011) The Th/La and Sm/La conundrum of the Tethyan realm lamproites. Earth and Planetary Science Letters, 301(3-4), 469–478.

Topuz, G., Okay, A.I., Altherr, R., Satir, M., and Schwarz, W.H. (2008) Late Cretaceous blueschist facies metamorphism in southern Thrace (Turkey) and its geodynamic implications. Journal of Metamorphic Geology, 26(9), 895–913.

Tribuzio, R., and Giacomini, F. (2002) Blueschist facies metamorphism of peralkaline rhyolites from the Tenda crystalline massif (northern Corsica): evidence for involvement in the Alpine subduction event? Journal of Metamorphic Geology, 20(5), 513–526.

Tribuzio, R., Messiga, B., Vannucci, R., and Bottazzi, P. (1996) Rare earth element redistribution during high-pressure-low-temperature metamorphism in ophiolitic Fe-gabbros (Liguria, northwestern Italy): Implications for light REE mobility in subduction zones. Geology, 24(8), 711.

Tsujimori, T., and Ernst, W.G. (2014) Lawsonite blueschists and lawsonite eclogites as proxies for palaeo-subduction zone processes: a review. Journal of Metamorphic Geology, 32(5), 437–454.

Tsujimori, T., Sisson, V., Liou, J., Harlow, G., and Sorensen, S. (2006) Very-low-temperature record of the subduction process: A review of worldwide lawsonite eclogites. Lithos, 92(3-4), 609–624.

Turner, S., Hawkesworth, C., van Calsteren, P., Heath, E., Macdonald, R., and Black, S. (1996) U-series isotopes and destructive plate margin magma genesis

in the Lesser Antilles. Earth and Planetary Science Letters, 142(1), 191–207.
Ueno, T. (1999) REE-bearing sector-zoned lawsonite in the Sanbagawa pelitic schists of the eastern Kii Peninsula, central Japan. European Journal of Mineralogy, 11(6), 993–998.
Ukar, E. (2012) Tectonic significance of low-temperature blueschist blocks in the Franciscan mélange at San Simeon, California. Tectonophysics, 568–569(0), 154–169.
Ukar, E., and Cloos, M. (2015) Magmatic origin of low-*T* mafic blueschist and greenstone blocks from the Franciscan mélange, San Simeon, California. Lithos, 230, 17–29.
Usui, T., Kobayashi, K., Nakamura, E., and Helmstaedt, H. (2007) Trace element fractionation in deep subduction zones inferred from a lawsonite-eclogite xenolith from the Colorado Plateau. Chemical Geology, 239(3-4), 336–351.
Van Hinsbergen, D.J.J. (2010) A key extensional metamorphic complex reviewed and restored: the Menderes Massif of western Turkey. Earth-Science Reviews, 102(1-2), 60–76.
Van Westrenen, W., Blundy, J.D., and Wood, B.J. (2001) High field strength element/rare earth element fractionation during partial melting in the presence of garnet: Implications for identification of mantle heterogeneities. Geochemistry, Geophysics, Geosystems, 2(7), 223–235.
Vitale Brovarone, A., Alard, O., Beyssac, O., Martin, L., and Picatto, M. (2014) Lawsonite metasomatism and trace element recycling in subduction zones. Journal of Metamorphic Geology, 489–514.
Volkova, N.I., and Budanov, V.I. (1999) Geochemical discrimination of metabasalt rocks of the Fan–Karategin transitional blueschist/greenschist belt, South Tianshan, Tajikistan: seamount volcanism and accretionary tectonics. Lithos, 47(3-4), 201–216.
Volkova, N.I., Stupakov, S.I., Babin, G.A., Rudnev, S.N., and Mongush, A.A. (2009) Mobility of trace elements during subduction metamorphism as exemplified by the blueschists of the Kurtushibinsky Range, Western Sayan. Geochemistry International, 47(4), 380–392.
Wang, Y., Prelević, D., Buhre, S., and Foley, S.F. (2017) Constraints on the sources of post-collisional K-rich magmatism: The roles of continental clastic sediments and terrigenous blueschists. Chemical Geology, 455, 192–207.
Wehrmeister, U., Jacob, D.E., Soldati, A.L., Loges, N., Häger, T., and Hofmeister, W. (2011) Amorphous, nanocrystalline and crystalline calcium carbonates in biological materials. Journal of Raman Spectroscopy, 42(5), 926–935.
Whitney, D.L., Teyssier, C., Seaton, N.C.A., and Fornash, K.F. (2014) Petrofabrics of high-pressure rocks exhumed at the slab-mantle interface from the "point of no return" in a subduction zone (Sivrihisar, Turkey). Tectonics, 33, 2315–2341.
Winchester, J.A., and Floyd, P.A. (1976) Geochemical magma type discrimination: application to altered and metamorphosed basic igneous rocks. Earth and Planetary Science Letters, 28(3), 459–469.
Wood, D.A. (1980) The application of a Th Hf Ta diagram to problems of tectonomagmatic classification and to establishing the nature of crustal contamination of basaltic lavas of the British Tertiary Volcanic Province. Earth & Planetary Science Letters, 50(1), 11–30.
Xia, Q.-X., and Zhou, L.-G. (2017) Different origins of garnet in high pressure to ultrahigh pressure metamorphic rocks. Journal of Asian Earth Sciences, 145, 130–148.
Xiao, Y., Niu, Y., Li, H., Wang, H., Liu, X., and Davidson, J. (2014) Trace element budgets and (re-)distribution during subduction-zone ultrahigh pressure metamorphism: Evidence from Western Tianshan, China. Chemical Geology, 365, 54–68.
Yaxley, G.M., and Green, D.H. (1998) Reactions between eclogite and peridotite: mantle refertilisation by subduction of oceanic crust. Schweizerische Mineralogische und Petrographische Mitteilungen, 78, 243–255.
Zhang, L., Wang, Q., and Song, S. (2009) Lawsonite blueschist in Northern Qilian, NW China: *P–T* pseudosections and petrologic implications. Journal of Asian Earth Sciences, 35(3-4), 354–366.
Zheng, B., Zhu, W., Jahn, B.M., Shu, L., Zhang, Z., and Su, J. (2010) Subducted Precambrian oceanic crust: Geochemical and Sr Nd isotopic evidence from metabasalts of the Aksu blueschist, NW China. Journal of the Geological Society, 167(6), 1161–1170.
Zhu, C.Y., Zhao, G., Sun, M., Liu, Q., Han, Y., Hou, W., Zhang, X., and Eizenhofer, P.R. (2015) Geochronology and geochemistry of the Yilan blueschists in the Heilongjiang Complex, northeastern China and tectonic implications. Lithos, 216-217, 241–253.

Manuscript received September 17, 2018
Manuscript accepted January 15, 2019
Manuscript handled by Gregory Dumon

Endnote:

[1]Deposit item AM-19-56818, Supplemental Material. Deposit items are free to all readers and found on the MSA website, via the specific issue's Table of Contents (go to http://www.minsocam.org/MSA/AmMin/TOC/2019/May2019_data/May2019_data.html).